

A DETAILED STUDY OF LASER ENHANCED IONIZATION
WITH ELECTROTHERMAL VAPORIZATION-FLAME
ATOMIZATION FOR TRACE ELEMENT ANALYSIS

By

KEN LYNN RITER

A DISSERTATION PRESENTED TO THE GRADUATE SCHOOL
OF THE UNIVERSITY OF FLORIDA IN PARTIAL FULFILLMENT
OF THE REQUIREMENTS FOR THE DEGREE OF
DOCTOR OF PHILOSOPHY

UNIVERSITY OF FLORIDA

1996

Dedicated to the loving memories of my mother, Namiko (Tamanaha) Riter (September 16, 1936 - July 9, 1983), and father, Roger Lynn Riter (July 12, 1945 - August 10, 1996). Without their love, encouragement, and support none of this would have been written.

ACKNOWLEDGMENTS

First, I would like to thank Dr. Jim Winefordner for the opportunity to research in his lab. Although I have learned much about laser spectroscopy in Jim's lab, his example of how to be a decent person and to treat others with respect is what will always be with me. I would like to thank Dr. Ben Smith for all of his advice and help in the lab. Setting up the instrumentation would have been an enormous task without Ben's help. I would like to thank Dr. Oleg Matveev for working with me and lending his expertise in laser enhanced ionization to the project. I have learned so much about LEI from Oleg in a very short period of time. Oleg's kindness, patience, and modesty allowed him to explain very difficult concepts rather easily.

I would like to thank Leah Mordoh and Wendy Clevenger for assisting with and performing many of the experiments for the LEIS of Mg. Others I would like to thank include Rob Guenard for his help with the ultrasonic nebulizer, Chester Eastman in the machine shop for building the new LEI burner, and all of the Winefordner and Harrison group members for their help and friendship. I would like to thank the National Institutes of

Health for funding this research (Grant # 5-R01-GM49638-03).

On a more personal note, I would like to thank my family for their love and encouragement. Thanks to Jon DeGnore, Dr. Bill Walden, and Dr. Wei Hang for being such good friends and making my stay in Gainesville enjoyable. Finally, I would like to thank my fiancée, Leah. Without her love and support, I do not know how I would have made it through these final few months.

All thanks be to God.

TABLE OF CONTENTS

ACKNOWLEDGMENTS	iii
LIST OF TABLES	viii
LIST OF FIGURES	ix
ABSTRACT	xii
CHAPTER 1	
INTRODUCTION	1
Absolute/Standardless Analysis	1
Analysis of Real Samples	5
Determination of Lead in Whole Blood	6
Intent of Dissertation	7
CHAPTER 2	
INTRODUCTION TO LASER ENHANCED IONIZATION	9
The Optogalvanic Effect	9
General Principles of LEI	10
Atomization of Sample	11
Excitation of Atoms	16
Ionization	20
Charge Collection	20
CHAPTER 3	
THEORY OF LASER ENHANCED IONIZATION	25
Introduction	25
Thermal Ionization	25
Processes Responsible for Thermal Ionization	27
Thermal Ionization Rate of an Atom in a Flame	29
Modeling of Laser Enhanced Ionization	30
Rate-Equation Formalism	30

Degree of Ionization for Two-Step	
Excitation	33
Density-Matrix Formalism	34
Detection of the Ionization Signal	38
One-Dimensional Approximation	39
Point Charge Model	39
Electrothermal Vaporization	40
Absolute Analysis	42

CHAPTER 4

REVIEW OF LASER ENHANCED IONIZATION	47
Analytical Performance of Flame-LEI	47
Limits of Detection and Sensitivities	47
Noise and Interferences	58
Applications of LEI to Real Samples	61
Determinations Without Interferant Removal	62
Determinations With Interferant Removal	66
Hybrid Techniques and Non-Flame Atom Reservoirs	71
Electrothermal Vaporizers	71
Hybrid Combinations of Flame and	
Electrothermal Vaporizers	74
LEI in the Inductively Coupled Plasma	79
Other Methods and Reservoirs	80

CHAPTER 5

EXPERIMENTAL	83
LEI	83
Burners	83
Graphite Furnace	88
Procedure and Conditions	97
Flame Gas Flows, Velocity, and Temperature	103
Noise Study	105
Fluorescence Dip and Fluorescence Profile of Flame	108
Transport Efficiency	113
Transimpedance Amplifier Calibration	118
Atomization Efficiency Measurement	119

CHAPTER 6

RESULTS AND DISCUSSION	124
LEI of Magnesium	124
Magnesium As Analyte	124
Mg LEI Signal	127
System Parameter Optimizations for Old Burner	

Design	130
Flame Profile With Old Burner	138
Analytical Curve With Old Burner	138
New Burner Design	145
System Parameter Optimizations With New Burner	148
Flame Profile With New Burner	157
Matrix Modifier/Carrier	166
Analytical Curve With New Burner	169
Flame Temperature and Flame Gas Velocity With the New Burner	174
Absolute Analysis	176
Vaporization Efficiency	176
Transport Efficiency	176
Probing Efficiency	178
Detection Efficiency	186
Atomization Efficiency	187
LEI of Lead	190
Excitation Scheme for Lead	190
Carrier	191
Calibration Behavior	200
CHAPTER 7	
CONCLUSIONS	202
Absolute Analysis	202
Pb in Blood	203
Future Work	203
REFERENCES	205
BIOGRAPHICAL SKETCH	216

LIST OF TABLES

<u>Table</u>	<u>page</u>
1. LEI limits of detection	48
2. Graphite furnace temperature program for magnesium	99
3. Graphite furnace temperature program for lead in blood	102
4. Values used for flame temperature calculation . .	175
5. Mg concentration in different cotton samples . .	177
6. Enhancement of LEI signal for different two-step excitation schemes for lead	192

LIST OF FIGURES

Figure	page
1. Processes needed for laser enhanced ionization spectrometry	13
2. Typical experimental setup for flame-LEI	15
3. Typical excitation schemes for LEI spectroscopy, a) one-step excitation using visible light, b) one-step excitation using ultraviolet light, c) two-step excitation (direct), d) two-step excitation (indirect), and e) three-step excitation	19
4. Various electrode arrangements used for LEI spectroscopy, a) split-cathode rod arrangement, b) split-cathode plate arrangement, c) water-cooled, immersed cathode arrangement, d) water-cooled coiled cathode arrangement	22
5. Schematic representation of various excitation and deexcitation processes in a three-level atom: n_1 , n_2 , and n_3 are the number densities of the three levels, respectively; k_{21} is the sum of the collisional deexcitation and spontaneous emission rates between levels 2 and 1; k_{12} is the collisional excitation rate between levels 1 and 2; $k_{3,100}$ ($k_{2,100}$) is the collisional ionization rate from level 3 (2); $B_{12}U_v(v_{12})$ ($B_{23}U_v(v_{23})$) and $B_{21}U_v(v_{21})$ ($B_{32}U_v(v_{32})$) are the absorption and stimulated emission rates and $U_v(v_{21})$ ($=U_v(v_{12})$) and $U_v(v_{23})$ ($=U_v(v_{32})$) are the spectral irradiances of the laser light	32
6. Block diagram of the experimental setup for LEIS	85
7. First burner design used for LEIS	87

8. Diagram of new burner design with relative position of the high voltage electrode and laser beams	90
9. Detailed drawing of the new burner design	92
10. Cut-away view of the graphite furnace showing the tantalum sample extraction interface	96
11. Sketch of laboratory constructed ultrasonic nebulizer used	107
12. Block diagram of experimental setup for monitoring of both fluorescence and LEI signals .	112
13. Sketch of experimental setup for transport efficiency measurement	116
14. Block diagram of the experimental setup for the determination of the atomization efficiency for Mg by atomic absorption	122
15. Oscilloscope trace of the laser beam timing . . .	126
16. Typical LEI signal for magnesium with older burner	129
17. Argon flow rate optimization for Mg with older burner	133
18. Burner-to-electrode distance optimization for Mg with older burner	135
19. Applied voltage optimization for Mg with older burner	137
20. Horizontal profile of the flame with the older burner	140
21. Analytical curve for Mg with the older burner . .	142
22. Log-Log plot of the analytical curve of Figure 21	144
23. Noises for the hydrogen/air and acetylene/air flames with the older burner design	147
24. Comparison of the noises for the new and old burner designs	150

25. Argon flow rate optimization with new burner . .	152
26. Acetylene flow rate optimization with new burner	154
27. Air flow rate optimization for new burner	156
28. Burner-to-electrode distance optimization for new burner	159
29. Electrode voltage optimization with new burner .	161
30. Horizontal profile of Mg atoms in flame with new burner	163
31. Fluorescence profile of Mg atoms in the flame with the new burner	165
32. LEI signal for xylene while scanning dye laser for λ_1	168
33. Effect of methanol on LEI signal for Mg	171
34. Analytical curve for Mg with new burner and methanol	173
35. Mg LEI signal with increasing laser repetition rate	181
36. Dye laser conversion efficiency with increasing laser repetition rate for λ_1	183
37. Dye laser conversion efficiency with increasing laser repetition rate for λ_2	185
38. Analytical curve for aqueous lead standards with and without NaCl addition	194
39. Log-Log plot of analytical curves for aqueous lead and blood lead	197
40. Analytical curve for diluted blood lead standards	199

Abstract of Dissertation Presented to the Graduate School
of the University of Florida in Partial Fulfillment of the
Requirements for the Degree of Doctor of Philosophy

A DETAILED STUDY OF LASER ENHANCED IONIZATION
WITH ELECTROTHERMAL VAPORIZATION-FLAME
ATOMIZATION FOR TRACE ELEMENT ANALYSIS

By

Ken Lynn Riter

December 1996

Chairperson: James D. Winefordner
Major Department: Chemistry

A system coupling electrothermal vaporization with flame-laser enhanced ionization (ETV-FL-LEI) was examined for the possibility of "absolute" analysis. For a method to be considered absolute, analytical matrix interferences must be eliminated, the stability of the calibration over time must be established, and the theoretical equation relating the signal to the quantity of analyte must be known. For our system, the LEI signal for magnesium is equal to the product of the Faraday number (96,485 C/mol), moles of Mg, and overall system efficiency. In our case, the overall system efficiency is the product of the vaporization efficiency of the ETV, the transport efficiency of Mg from the ETV to the flame, the atomization efficiency of Mg in the flame, the probing

efficiency of the laser beams, and the detection efficiency. Ideally, these efficiencies should be unity. However, it was found that all of these except the vaporization efficiency was less than unity. Also, the LEI signal deviated from linearity at low Mg concentrations and required the addition of a matrix modifier to restore the signal. This indicates a dependence of the LEI signal on the sample matrix. Therefore, ETV-FL-LEI should not be considered an absolute method.

A second project involved the application of our ETV-FL-LEI system to the determination of lead concentration in whole blood. Blood standards from the Centers for Disease Control (CDC) and the National Institute of Standards and Technology (NIST) were diluted 21:1 with ultra pure water and analyzed. Good agreement was found between the CDC and NIST standards. A linear analytical curve was obtained with a detection limit (3σ) of $8.9 \times 10^{-3} \mu\text{g/dL}$ (890 fg absolute) for lead in whole blood. This compares favorably with other current methods for blood lead determinations including isotope dilution inductively coupled plasma mass spectrometry (ID-ICP-MS) and graphite furnace atomic absorption spectrometry (GFAAS).

CHAPTER 1 INTRODUCTION

Absolute/Standardless Analysis

There are no analytical procedures which are "absolute" in the strictest sense of the word, because to analyze absolutely - i.e. without any presuppositions - it would be necessary to identify the atoms and the molecules of the sample, to sort them out, and to count them individually and completely [1].

However, if a theoretical expression is known for the function relating the signal to the absolute quantity of analyte present that is sufficiently reliable to allow a direct calculation of the quantity of analyte from a single measurement, then this method is called "an absolute method of analysis" [2]. The most complete program for the development of absolute methods of analysis includes [2]: (1) elimination of analytical matrix interferences, (2) stabilization of the calibration over time, and (3) theoretical calculation of the calibration based on fundamental parameters and actual measurement conditions. This should be distinguished from

"standardless" analysis where the calibration curve is stable over time. Therefore, once the system has been calibrated for a particular sample, the calibration should need to be checked only occasionally (such as once every 8 hours) with a standard (concentration = 100 to 1000 times the limit of detection).

Many classical methods, such as precipitation reactions, titrimetry, and coulometry, are considered absolute. When considering modern instrumental methods for absolute analysis, usually atomic absorption, where relative measurements are made, is considered the best candidate rather than emission or fluorescence procedures where absolute radiometric measurements are required. According to L'vov [2], this is not surprising since the atomic absorption method of measuring the analytical signal is free from many of the uncontrolled or difficult-to-control factors typical of emission/fluorescence methods. Also, the stability and consistency of calibration for modern graphite furnace atomic absorption spectroscopy (GF-AAS) have brought GF-AAS close to achieving absolute analysis. However, the sensitivity of GF-AAS, although high, is still well within the possibility of preparation of accurate standard reference solutions with minimal contamination and loss problems. In this respect, absolute analysis by GF-AAS will most likely never be a necessity. However, GF-AAS is very amenable to standardless analysis

because of the reproducibility and consistency of the calibration. Electrothermal vaporization-inductively coupled plasma-mass spectrometry has achieved, in some cases, low or even sub-femtogram detection limits. However, it is essential that standard samples or solutions be used for calibration, since the transport efficiencies of analyte ions are unknown and vary significantly with analyte type, matrix type, gas flow rates, sampling cone and skimmer cone geometries and electrostatic lens configuration and conditions.

Laser induced fluorescence with graphite furnace atomization (GF-LIF) is one of the most sensitive methods for trace element analysis. However, absolute analysis by GF-LIF involves a difficult and time consuming calibration process relating the signal level to the mass of the analyte and requires corrections for laser induced ionization, thermal ionization, and matrix background, and evaluation of or knowledge of the diffusion coefficient of analyte atoms at the furnace atomization temperature.

Analytical methods based upon ionization are potentially the best candidates for absolute analysis. Ions can be produced with great selectivity and, once an ion is produced, the probability of detection is generally high. Moreover, most of the complexities associated with absolute fluorescence measurements are avoided; the relationship between amount of analyte and the measured signal is substantially simpler. A

new analytical approach using laser enhanced ionization with sub-fg (and sub-pg/mL) detection limits has been described by Smith et al. [3,4] which shows great promise as a standardless or absolute method. This method involves coupling of a graphite furnace for sample vaporization with an acetylene/air flame for laser enhanced ionization (LEI) detection. In essence, this method can be considered as the analog of coulometry (i.e. each atom will produce a charge of 1.6×10^{-19} C or 96,487 C/mol). It is hoped that the combination of high sensitivity and simplicity of detection will make LEI a good candidate for absolute analysis.

There are several fields in which extreme sensitivity (sub-fg) combined with absolute analysis would be useful since the preparation of standards at very low analyte concentrations is difficult because of sample loss and contamination problems. This makes the development of an absolute analytical protocol a pressing need [5]. In medical research, the determination of the microdistribution of trace metals in μg amounts of human tissues is essential and concentration levels at or below pg/g are common [6]. However, the preparation of standards is difficult or impossible because of the complexity of the sample matrix. Similar detection capability is required for the determination of trace elements in small amounts of solid samples of

interest in criminalistic, expert legal, and forensic medical cases [7]. In situations where the preparation of hazardous standards needs to be avoided, e.g. the analysis of radioactive species, a means of quantitation using an absolute approach would be desirable. These examples are indicative of the situations where absolute analysis by graphite furnace-flame-LEI spectroscopy would be desirable: (i) when the quantities of sample are limited and (ii) when standards are difficult or impossible to prepare due to the very low concentrations being used, the difficulty of simulating very complex sample matrices, or the danger of handling hazardous analytes.

Analysis of Real Samples by LEI Spectrometry

Laser enhanced ionization spectrometry (LEIS) is a sensitive technique for trace element analysis and has become well established since its discovery in 1976 [8]. Unfortunately, the application of LEIS has been limited mostly to simple aqueous systems because of ionization interferences encountered in complex matrices. Thus, the application of LEIS to complex real samples, such as biological fluids and environmental samples, has remained largely undeveloped.

The combination of the graphite furnace, used as an electrothermal vaporizer (ETV), with a flame for LEI detection

has many advantages for the analysis of real samples. By separation of the graphite furnace vaporization and LEI detection processes, this system overcomes the problems of thermionic emission from the graphite tube and poor collisional ionization encountered with LEIS in the graphite furnace. This system also allows for the removal of many interfering matrix species by temperature programming of the graphite furnace. As a result, ionization interferences that have plagued LEIS of real samples may be reduced or even eliminated.

Determination of Lead in Whole Blood

Since the Centers for Disease Control (CDC) lowered its pediatric level of concern for blood lead to 10 $\mu\text{g/dL}$ in 1991, there has been increased interest in more sensitive methods for the determination of lead concentrations in blood. There also exists a need in research laboratories for accurate and precise measurements of substantially lower blood lead levels ($\ll 10 \mu\text{g/dL}$) to establish the levels for chronic lead toxicity in humans [9]. Some studies indicate that there may be no threshold for lead toxicity in humans [10,11], and so the need for more sensitive methods for determining blood lead levels is clear.

Isotope dilution inductively coupled plasma mass

spectrometry (ID-ICP-MS) and graphite furnace atomic absorption spectrometry (GFAAS) are both methods currently used to measure low levels of lead in blood. However, both of these methods require extensive sample preparation with a matrix modifier, and have detection limits of only around 1 $\mu\text{g}/\text{dL}$ for lead in whole blood [12,13]. With the combination of graphite furnace with flame-LEIS, little sample preparation is needed (21:1 dilution with ultra pure water) unlike with ID-ICP-MS and GFAAS. This not only reduces the complexity of sample preparation but also reduces sample contamination from matrix modifiers. This becomes especially important at very low blood lead levels, so improved detection limits may be expected. Another advantage of the ETV-LEIS combination is the high sensitivity afforded by LEIS.

Intent of Dissertation

The aim of the present work was to satisfy the third condition for absolute analysis (stated earlier) by characterizing the efficiencies associated with our experimental setup (consisting of the combination of a graphite furnace with an acetylene/air flame for LEI detection) to obtain the theoretical equation relating the analyte quantity to the LEI signal. This equation and the efficiencies will be discussed in more detail in Chapter 2.

A second objective was to explore the possibility of applying this technique to the analysis of real samples with complex matrices. We chose to analyze lead concentrations in a blood matrix.

CHAPTER 2 INTRODUCTION TO LASER ENHANCED IONIZATION

The Optogalvanic Effect

The optogalvanic effect (OGE) is the term for the process whereby the collisional ionization rate for an element is enhanced by optical excitation to a higher electronic energy state [8,14]. This mechanism was first postulated by Foote and Mohler in 1925 [15]. The first purely optical/collisional effect, however, was not actually observed until 1928 by Penning [16]. Penning observed the effect as a change in the voltage drop across a neon discharge when illuminated by a second neon discharge.

Unfortunately, optical enhancement of collisional ionization is too weak of an effect to be seen in usual atom reservoirs with conventional light sources. Therefore, it would not be until the advent of tunable lasers that the OGE could be easily observed and used as a spectroscopic method.

In 1976, researchers at the National Bureau of Standards (NBS, now the National Institute of Standards and Technology, NIST) decided to investigate the hollow cathode lamp as a reservoir for laser induced fluorescence (LIF) after disappointing results for LIF in a flame [17]. These researchers fortuitously discovered a change in the voltage

across the hollow cathode lamp when the dye laser was tuned to an electronic transition of one of the atomic species in the discharge [14]. Shortly afterwards, the same group decided to look for a related effect in flames. The effect was observed and a sub-ppb detection limit for sodium, equivalent to their results with LIF in a flame, was quickly obtained [8].

The term, laser enhanced ionization (LEI), was first introduced in 1978 by the group at NBS [18]. Today, LEI is used to describe the optogalvanic effect in flames and other reservoirs except discharges. OGE or optogalvanic spectroscopy (OGS) is now used exclusively for phenomena taking place in discharges.

General Principles of LEI

Laser-enhanced ionization spectrometry (LEIS) can be defined as a spectroscopic method where an enhancement in the normal collisional (thermal) ionization is obtained by optical excitation of the atoms under study by resonant laser light. This enhancement is detected as a change in the current passing through a medium (atom reservoir) between two electrodes at different potentials.

LEI can be broken down into four distinct processes: atomization of the sample, optical excitation of the analyte atoms by resonant laser light, collisional ionization of the

excited atoms, and collection of the charges produced (Figure 1).

Atomization of Sample

The conversion of the sample into an atomic vapor or atomization of the sample is dependent upon the particular characteristics of the atom reservoir used. To date, many different atom reservoirs have been used for LEI including atmospheric flames, graphite furnaces, and inductively coupled plasmas (ICPs). However, the large majority of LEI studies have been done in atmospheric flames. This is because of the combination of good qualities that flames exhibit for atomization, ionization, and the detection processes. A typical flame-LEI setup is shown in Figure 2 and consists of a flame, laser system, electrodes, and electronic detection equipment.

In conventional flame-LEI, the sample is aspirated by a pneumatic nebulizer into a spray chamber. The sample leaves the spray chamber as a spray or mist of fine droplets and enters the flame. The flame heats this spray and causes the solvent to vaporize leaving dry aerosol particles. Further

Figure 1. Processes needed for laser enhanced ionization spectrometry [19]

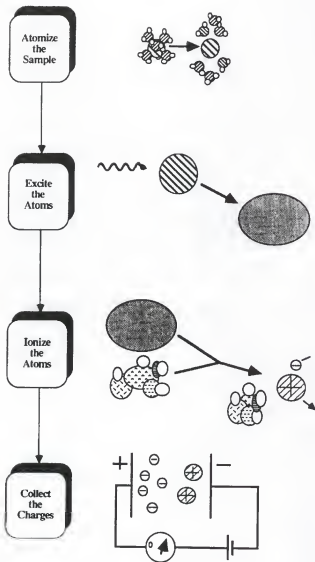
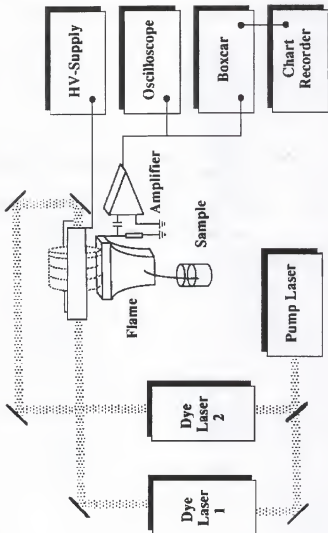


Figure 2. Typical experimental setup for flame-LEI [19]



heating in the flame volatilizes these dry aerosol particles producing atomic, molecular, and ionic species.

Many different flames have been used for LEIS including acetylene-based flames such as C_2H_2/air and C_2H_2/N_2O and hydrogen-based flames such as H_2/N_2O , and $H_2/O_2/Ar$. The cooler hydrogen-based flames have little flame-ion production so the background noise from the flame is low. However, the flame temperature and flame composition have been found to be the most important factors in obtaining strong LEI signals, because these factors greatly affect the atomization efficiency. Therefore, the hotter acetylene-based flames are most commonly used as atomic reservoirs in LEI. On the other hand, if the flame temperature is too high, thermal ionization of the analyte may be considerable resulting in poor detection limits for atomic LEI. The most common flame used for LEI has been the air/acetylene flame in which a large number of elements can be conveniently analyzed. Hotter flames, such as C_2H_2/N_2O , are mostly used for refractory elements.

Excitation of Atoms

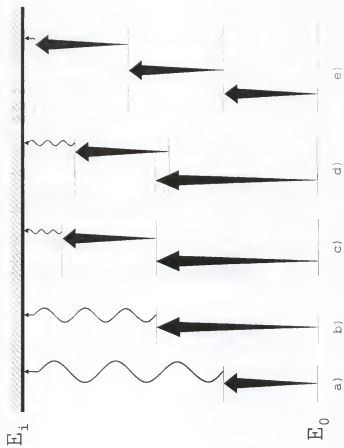
Optical excitation of the analyte atoms is usually performed by a pulsed dye laser. The dye laser may be pumped by a variety of sources including flashlamps, Nd:YAG, excimer, and N_2 lasers. Continuous-wave (cw) lasers have been used infrequently for LEI because cw techniques are often too

complicated for analytical applications. This is mostly due to the ability of pulsed laser sources to produce much higher intensity light, especially in the ultra-violet region. Another advantage of pulsed lasers for LEI is that the excess charge created can be collected during a shorter period of time, which reduces the influence of background current noise.

Flashlamp-pumped dye lasers usually have pulse durations in the microsecond range while excimer, Nd:YAG, and N_2 -pumped dye lasers usually have pulse durations around 5-20 ns. Pulse energies vary typically from 0.1 to 100 mJ in the visible and 1 mJ to 10 mJ in the ultra-violet region depending on the laser system, dyes, and crystals used. The wavelength region covered by dye laser systems typically ranges from 220 nm to 1000 nm. Repetition rates used are normally around 5-100 Hz.

Many different excitation schemes may be used for LEI spectroscopy, some of which are shown in Figure 3. One-step excitation using either visible or ultra-violet light has been used extensively in flame-LEIS. For elements that are more easily ionized, a single-step scheme is sufficient to achieve low limits of detection. However, for many elements, it is favorable to use a two-step excitation scheme. Most two-step schemes share an intermediate level although this is not necessary if the upper level of the first step and the lower level of the second step are sufficiently coupled by

Figure 3. Typical excitation schemes for LEI spectroscopy, a) one-step excitation using visible light, b) one-step excitation using ultraviolet light, c) two-step excitation (direct), d) two-step excitation (indirect), and e) three-step excitation.



collisions. The addition of the second step usually results in a significant increase in the signal strength (up to three orders of magnitude) compared to one-step excitation. Three-step excitation schemes have also been used but are not common in flame-LEIS.

Ionization

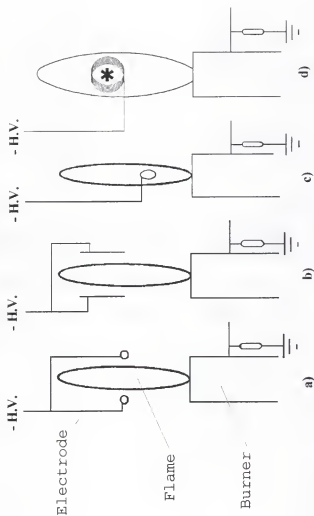
The common atomic reservoirs (flames, furnaces, and plasmas) result in thermal ionization. Most atoms ionize through collisions with thermally excited molecules in the reservoir. Therefore, the thermal ionization rate depends on the reservoir constituents, temperature of the medium, and the ionization potential of the element of interest.

When an element is excited by laser radiation, the atomic population of that element is greatly altered. Excited atoms are more easily ionized by collisions than those in the ground state, so an increased ionization rate results.

Charge Collection

The additional charges produced by optical excitation are collected by applying an electrical field across the flame (or other atomic reservoir) using an electrode arrangement and measuring the current change. Many different electrode arrangements have been used, some of which are shown in Figure 4.

Figure 4. Various electrode arrangements used for LEI spectroscopy, a) split-cathode rod arrangement, b) split-cathode plate arrangement, c) water-cooled, immersed cathode arrangement, d) water-cooled coiled cathode arrangement.



In all four schemes, the burner head acts as the anode and is connected to the detection electronics. In the split-cathode rod arrangement (Figure 4a), two metal rods are positioned on opposite sides of the flame and biased to the same negative high voltage with respect to the burner head. This arrangement was found to be very sensitive to easily ionized matrix species [20,21]. This led to the development of the split-cathode plate arrangement (Figure 4b) which was used for several years [22,23]. This was the case because of its stable electric field distribution in the flame, relatively high contamination resistance, and long lifetime.

The stainless steel, water-cooled, immersed cathode arrangement (Figure 4c) was developed to locate the cathode as close to the laser excitation zone as possible [24]. The maximum signal strength and optimal resistance to electrical matrix interference should occur with the laser excitation as close to the cathode as possible. This electrode is also easy to fabricate, robust, and contributes negligible memory effects. The saturation current is also reduced with respect to that of the split-cathode plate, which results in a lower background current. The water-cooled coiled cathode (Figure 4d) has equivalent sensitivity to the immersed cathode and appears to have even greater resistance to easily ionized matrix species [25].

Depending on other experimental parameters such as electrode configuration, the applied voltage varies from about 300 V to ~3000 V. The current drawn through the flame is usually in the μA range and the amount of charge detected is in the fC range or larger. A typical LEI signal has a duration of 300 ns up to 1 μs . The very small LEI current is directed through a current-to-voltage amplifier which is usually placed very close to the flame to minimize radio frequency noise from the pulsed laser. The d.c. current is usually filtered out using a d.c. blocking capacitor.

The current pulse is detected synchronously using a boxcar integrator with pulsed laser excitation or a lock-in amplifier with a chopped continuous wave laser. The signal is then collected and processed by a computer.

CHAPTER 3

THEORY OF LASER ENHANCED IONIZATION

Introduction

The basic principle of laser enhanced ionization (LEI) is to enhance the existing thermal ionization rate in the flame (or alternate atom reservoir) by optical (laser) excitation and then to detect this increase in the ionization rate as an increase in the current passing through the flame between two electrodes. A discussion of the theory for two-step LEI in flames will be covered here. A more general and in-depth discussion of LEI theory is given by Axner and Rubinsztein-Dunlop [26] and Travis and Turk [27].

Thermal Ionization

A combustion flame possesses a small but not always insignificant amount of thermal ionization [5]. If an atomic

system is retained in a flame, we can define a thermal ionization rate constant, $k_{th.ion}$, for each specific process in the flame. One such process is the collisional ionization between a species M and a thermally excited collisional partner X^* :



where M^+ is the positive ion, e^- is an electron, X is the deexcited collisional partner.

Similarly, there exists a recombination rate constant, $k_{recomb.}$, for the reverse process, given by:



When the system is in thermal equilibrium, the thermal ionization and recombination rates balance exactly. This enables us to write an expression for the relation between the concentration of the species M, its ions, and the electrons. This relation is known as the Saha equation [28] and is stated as:

$$[M^+] [e^-] = K_{ion} [M] \quad (3)$$

where K_{ion} is the ionization constant given by:

$$K_{ion} = \frac{k_{th.ion}}{k_{recomb}} \quad (4)$$

It should be noted that although a third body (collision partner) is required for the ionization and recombination processes and the rates for each of these processes is dependent upon the concentration of the third body, the ionization constant (and degree of ionization of the atomic system) is independent of the concentration of this third body as long as thermal equilibrium conditions prevail in the flame.

As has already been mentioned, in LEI, an electric field is applied to the volume of interaction within the flame to separate the created charges and make detection of those charges possible. Consequently, the electric field will minimize recombination from occurring at any significant rate. Therefore, the only remaining process will be thermal ionization, so the Saha equation is no longer valid.

Processes Responsible for Thermal Ionization

In a flame, a variety of different interactions between atoms, molecules, and light can take place. The major processes that lead to ionization can be divided into physical and chemical ionization processes. The physical processes and be further divided into collisional and radiative ionization processes.

Collisional ionization processes are most often considered to be responsible for ionization of atoms in

flames. An example would be the collisional ionization of sodium atoms in the flame:



where X represents any flame molecule [5,29].

Radiative ionization processes are usually photoionization processes where atoms are irradiated with high intensity, short wavelength light which results in the ejection of an electron, such as:



or by the interaction between blackbody radiation and excited atoms.

Chemical ionization processes are most easily characterized as those in which the formation of a new chemical bond takes place. Most alkaline earth atoms are believed to ionize in this way. Associative ionization, such as for the calcium atom:



represents such a process. There are also many charge distribution processes that may be of importance since they can constitute one reaction in a chain leading to a net ionization rate.

Thermal Ionization Rate of an Atom in a Flame

To model thermal ionization, some assumptions must be made. It is assumed that collisional ionization dominates other ionization processes in the flame. It is also assumed that the flame, with all of its atomic and molecular species, is in a state of thermal equilibrium. This implies that the concept of detailed balance between all atomic levels is valid. In other words, the atomic energy levels are populated according to Boltzmann's distribution:

$$n_i = \frac{g_i \exp(-E_i/kT)}{Z} n_{\text{atom}} \quad (8)$$

where n_i is the population of the i^{th} level (m^{-3}), g_i is the degeneracy of the i^{th} level, E_i is the energy of the i^{th} level, n_{atom} is the total number density of neutral atoms (m^{-3}), and Z is the electronic partition function:

$$Z = \sum_i g_i \exp(-E_i/kT) \quad (9)$$

where k is the Boltzmann constant and T is the flame temperature.

However, the thermal ionization rate will be overestimated unless we assume that the condition of detailed balance is not valid for the highest lying states in the atom. If we assume that detailed balance is only valid for states up

to a certain level, then the thermal ionization rate, dn_{ion}/dt ($\text{m}^{-3} \text{s}^{-1}$), can be expressed by:

$$\frac{dn_{\text{ion}}}{dt} = \left(\frac{8kT}{\pi\mu} \right)^{1/2} \sigma_{\text{ion}}^X \frac{\exp(-E_{\text{ion}}/kT)}{Z} n_X \sum_{i=1}^{i_{\text{ion}}} g_i n_{\text{atom}} \quad (10)$$

where μ is the reduced mass of the system [$\mu = m_{\text{atom}} m_X / (m_{\text{atom}} + m_X)$, where m_{atom} and m_X are the masses of the atom under consideration and collision species X, respectively], σ_{ion}^X is the ionization cross section for the species X, E_{ion} is the energy of the ionization limit, and n_X is the concentration of species X.

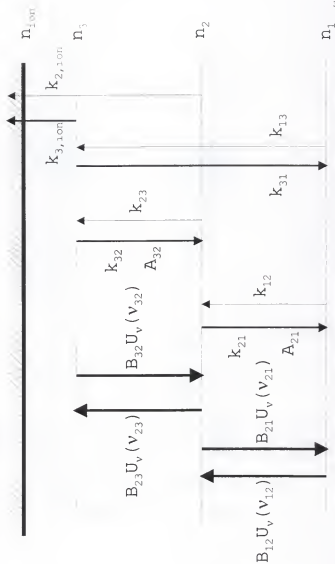
Although, with the above simplification, the thermal ionization rate depends greatly upon what cutoff level is chosen, the relationship between the enhanced ionization rate due to laser excitation and the thermal ionization rate is not very sensitive to the specific cutoff level chosen.

Modeling of Laser Enhanced Ionization

Rate-Equation Formalism

Let us assume a three-level atom illuminated by two laser beams. For simplicity, it is assumed that the atoms consist of only three bound levels (see Figure 5) among which laser

Figure 5. Schematic representation of various excitation and deexcitation processes in a three-level atom: n_1 , n_2 , and n_3 are the number densities of the three levels, respectively; k_{21} is the sum of the collisional deexcitation and spontaneous emission rates between levels 2 and 1; k_{12} is the collisional excitation rate between levels 1 and 2; $k_{3,100}$ ($k_{2,100}$) is the collisional ionization rate from level 3 (2); $B_{12}U_\nu(v_{12})$ ($B_{23}U_\nu(v_{23})$) and $B_{21}U_\nu(v_{21})$ ($B_{32}U_\nu(v_{32})$) are the absorption and stimulated emission rates and $U_\nu(v_{21})$ ($=U_\nu(v_{12})$) and $U_\nu(v_{23})$ ($=U_\nu(v_{32})$) are the spectral irradiances of the laser light.



excitation takes place in two steps, weakly coupled to an ionization continuum.

Degree of Ionization for Two-Step Excitation

The degree of ionization here is defined as the fraction of atoms in the interaction volume that ionize during the laser pulse. The expression for the degree of ionization is considerably simplified by assigning an effective collisional ionization rate from the uppermost laser-coupled level, $k_{3,ion}^{eff}$. With these assumptions, the ionization rate can be written as:

$$\frac{dn_{ion}^{on}}{dt} = C_3^{on} k_{3,ion}^{eff} (n_{tot} - n_{ion}) \quad (11)$$

where

$$C_3^{on} = (C_3^{on})_{sat} \frac{B_{12}U_v(v_{12})B_{23}U_v(v_{23})}{(B_{12}U_v(v_{12})+a)(B_{23}U_v(v_{23})+b)+d} \quad (12)$$

$$(C_3^{on})_{sat} = \frac{g_3}{g_1+g_2+g_3} \quad (13)$$

$$a = (C_3^{on})_{sat} k_{31} + (C_2^{on})_{sat} k_{21} \quad (14)$$

$$b = \frac{(C_3^{on})_{sat}}{(C_2^{on})_{sat}} (k_{31} + k_{32}) \quad (15)$$

$$d = [(C_3^{on})_{sat}]^2 (k_{31} + k_{32}) \left(k_{21} - \frac{k_{31}}{(C_2^{on})_{sat}} \right) \quad (16)$$

$$(C_2^{\text{off}})_{\text{sat}} = \frac{g_2}{g_1 + g_2} \quad (17)$$

$$(C_2^{\text{on}})_{\text{sat}} = \frac{g_2}{g_1 + g_2 + g_3} \quad (18)$$

n_{tot} is the total number density of the analyte (neutral atoms and ions), n_{ion} is the number density of analyte ions, and the designations of "on" and "off" refer to the second laser beam (λ_2) being on or off.

Time dependent solutions to these equations for an interaction time, τ , of laser light can then be readily expressed as:

$$n_{\text{ion}}^{\text{on}}(\tau) = \alpha_{\text{ion}}^{\text{on}}(\tau) n_{\text{tot}} \quad (19)$$

where $\alpha_{\text{ion}}^{\text{on}}$ represents the degree of ionization of the atomic system and can be expressed as:

$$\alpha_{\text{ion}}^{\text{on}}(\tau) = 1 - \exp(-C_3^{\text{on}} k_{3,\text{ion}}^{\text{off}} \tau) \quad (20)$$

Density-Matrix Formalism

The rate-equation formalism, however, is primarily valid only for one-step excitation so an effective model for two-step excitation is needed. Effects not taken into account are those primarily caused by intense light fields, such as two-

photon excitation and dynamic Stark broadening, splitting, and shifting. In order to account for these effects while keeping the model as simple as possible, a theory for LEI based on the density-matrix formalism was proposed by Axner et al. [26,30,31,32,33].

The density-matrix formalism of light and matter interactions and its theoretical assumptions have been discussed in detail in many sources previously [30,34,35,36,37,38,39,40,41,42,43]. Therefore, only a brief overview will be given here.

Assuming that the laser frequency profile is Lorentzian, the system of density matrix equations can be solved under steady-state conditions when the time dependencies of the level populations are neglected. The steady-state simplification is valid if the pulse duration is substantially longer than the inverse of the deexcitation collision rate. The following expressions result for the fractions of atoms excited, C_2^{DM} and C_3^{DM} (where $^{\text{DM}}$ denotes the Density Matrix formalism), for the density-matrix formalism:

$$C_2^{\text{DM}} = \frac{n_2}{n_{\text{atom}}} = \frac{1}{3} \frac{R_{12}(R_{23} + k_{31} + k_{32}) + (R_{13}(R_{12} + R_{23} + k_{32}))}{\bar{D}} \quad (21)$$

$$C_3^{\text{DM}} = \frac{n_3}{n_{\text{atom}}} = \frac{1}{3} \frac{R_{12}R_{23} + R_{13}(R_{12} + R_{23} + k_{21})}{\bar{D}} \quad (22)$$

where the denominator, \bar{D} , is given by:

$$\begin{aligned} \bar{D} = & R_{12}R_{23} + R_{13}(R_{12} + R_{23}) + \frac{2}{3}R_{12}(k_{31} + k_{32}) \\ & + \frac{1}{3}R_{23}(k_{21} + k_{31}) + \frac{1}{3}R_{13}(2k_{21} + k_{32}) + \frac{1}{3}k_{21}(k_{31} + k_{32}) \end{aligned} \quad (23)$$

and where R_{12} , R_{23} , and R_{13} are the excitation rates for the atoms given by:

$$R_{12} = \frac{(\omega_R^{12})^2}{2} \operatorname{Im} \left(\frac{4\Delta_{23}\Delta_{13} - (\omega_R^{12})^2 + (\omega_R^{23})^2}{D} \right) \quad (24)$$

$$R_{23} = \frac{(\omega_R^{23})^2}{2} \operatorname{Im} \left(\frac{4\Delta_{12}\Delta_{13} - (\omega_R^{23})^2 + (\omega_R^{12})^2}{D} \right) \quad (25)$$

$$R_{13} = -\frac{(\omega_R^{12})^2(\omega_R^{23})^2}{2} \operatorname{Im} \left(\frac{1}{D} \right) \quad (26)$$

$$D = 4\Delta_{12}\Delta_{23}\Delta_{13} - (\omega_R^{12})^2\Delta_{12} - (\omega_R^{23})^2\Delta_{23} \quad (27)$$

where $\operatorname{Im}()$ denotes the imaginary component, ω_R^{12} and ω_R^{23} are the Rabi flop frequencies and Δ_{12} , Δ_{23} , and Δ_{13} are the complex detunings given by:

$$\omega_R^{12} = [(\Lambda_{21}\lambda_{12}^{-3}I_{12}) / (2\pi\hbar c)]^{1/2} \quad (28)$$

$$\omega_R^{23} = [(\Lambda_{32}\lambda_{23}^{-3}I_{23}) / (2\pi\hbar c)]^{1/2} \quad (29)$$

$$\Delta_{12} = \omega_{12} - \Omega_{12} - i\gamma_{21} \quad (30)$$

$$\Delta_{23} = \omega_{23} - \Omega_{23} - i\gamma_{32} \quad (31)$$

$$\Delta_{13} = (\omega_{12} + \omega_{23}) - (\Omega_{12} + \Omega_{23}) - i\gamma_{31} \quad (32)$$

where ω_{12} and ω_{23} are the energy between the levels in angular frequency units, Ω_{12} and Ω_{23} are the angular frequencies (rad/s) of the laser light related to the wavelength by

$\Omega=2\pi c/\lambda$, and γ_{12} , γ_{13} , and γ_{23} are the "off-diagonal" decay rates between levels 1 and 2, 1 and 3, and 2 and 3, respectively, given by:

$$\gamma_{21}=\frac{1}{2}k_{21}+\gamma_c+\gamma_L \quad (33)$$

$$\gamma_{31}=\frac{1}{2}(k_{31}+k_{32})+\gamma_c+2\gamma_L \quad (34)$$

$$\gamma_{32}=\frac{1}{2}(k_{21}+k_{31}+k_{32})+\gamma_c+\gamma_L \quad (35)$$

where k_{21} , k_{31} , and k_{32} are the inelastic collision rates between the levels, γ_c is the elastic collision rate, and γ_L is the half-width half-maximum laser bandwidths in angular frequency units.

These equations are analyzed in more detail by Axner and Ljungberg [36]. Some of the main properties of these equations are briefly discussed below.

Computer simulations based on this theory reproduce the main features of experimental curves fairly well, although exact lineshapes and peak heights are not always satisfactorily reproduced [5]. In other words, there is a qualitative agreement between experiment and theory in predicting the LEI signal lineshapes. However, the quantitative agreement is still unsatisfactory and a refinement of the theory is required. Several studies have been published in the areas where the theory is not satisfactory [31,32,33,44,45,46], such as the description of

the properties of the laser light and the collisional broadening and ionization mechanisms. Consequently, these will not be discussed here.

It should be noted, however, that many assumptions were made in solving the density-matrix equations. Some of these approximations included: neglect of the mode structure of the laser light, assuming Lorentzian-shaped wings for the laser light, reduction of the system to a three-level non-degenerative system, and neglect of Doppler broadening, depletion, and the influence of other non-laser-connected levels. Consequently, the above theoretical model will not adequately describe experimental results in certain situations where these assumptions do not hold. However, in general, the theoretical model is more than adequate in most analytical situations.

Detection of the Ionization Signal

As has been noted by other authors [27,47], a good theory for LEI signal detection in the air/acetylene flame has remained largely underdeveloped. Therefore, a theory of LEI signal detection and optimization will not be presented in detail. A brief overview of the concepts and simple approaches to modeling the detection of natural and laser-

produced ions and electrons will be given.

One-Dimensional Approximation

A one-dimensional model of the distributions and dynamics of ions, electrons, and fields in flames has been described by Travis and Turk [27]. In this model, the only axis accommodated mathematically is perpendicular to the plane of the electrodes assuming that plate electrodes are used. Other assumptions include: the flame uniformly fills the space between the plates and that both the flame and laser light extend infinitely in the directions parallel to the plates (this results in a laser beam shape of a plane rather than a more realistic line).

Point Charge Model

The point charge model can be used to describe the LEI signal when pulsed laser excitation is used. This theory is described in detail elsewhere [48,49,50]. This model assumes that pulsed laser excitation instantaneously deposits charges (ions and electrons) in the flame. Travis and Turk [27] have written a computer program to numerically model the LEI signal by convolving the point charge model with charge distribution functions.

The simulated current vs voltage curves and experimental results for the air/acetylene flame (with the immersed electrode configuration) are not in good agreement. The

reasons for this have been discussed by Travis and Turk [27] and will not be presented here.

Therefore, there still exists a need for development of an adequate model for LEI signal detection in the air/acetylene flame and with the immersed electrode configuration. Many opportunities exist for the extension of the existing theory to higher dimensionalities and to different geometries.

Electrothermal Vaporization

Electrothermal vaporizers have been studied extensively for sample introduction into the inductively-coupled plasma (ICP) and other plasmas. A detailed theory for electrothermal vaporization and vapor transport has been described by others [51,52,53,54]. A brief discussion will be presented here.

The production of dry aerosols by high temperature processes, such as in the graphite furnace, is known as thermal dispersion. Once the vapor is produced, condensation of the vapor is needed for effective transport to the observation well. This can be attained by physical condensation of the vapor, vapor condensation on foreign particles, or chemical condensation of the vapor.

Physical condensation is the attainment of

supersaturation by cooling the vapor or vapor-gas mixture [52]. The simplest method of effective cooling is the mixing of vapor with a turbulent stream of cold gas. When condensation nuclei are generated by the vapor itself, the process is known as homogeneous nucleation or self-nucleation [55]. When a high concentration of stable nuclei is attained, condensation of vapor takes place on existing particles which is called heterogeneous condensation [55]. When a high concentration of fine particles is reached, their growth is governed by Brownian coagulation. Coagulation occurs when two particles collide and adhere to form a single particle.

The condensation of the vapor of a volatile analyte on the stable nuclei formed from another substance in the furnace is likely to take place under ETV conditions. If adequate mixing is achieved, a component of low volatility can increase the transport efficiency of a volatile analyte, even if the evaporated masses of the two components are equally small. Condensation of the analyte vapor can also take place on stable nuclei produced from organic substances as solid sample matrices or additives. In general, the condensation of analyte vapor on foreign particles of different origin is expected to be one of the most important processes in the ETV methods. It is also expected that this process enhances the transport efficiency of the analyte. In other words, a carrier effect will result.

Chemical condensation takes place when the vapor undergoes a reaction by which a compound is formed which is less volatile than the vaporized substance [40]. A good example of this is the formation of a metal oxide. Therefore, it should be kept in mind that the chemical form of the analyte vapor as released initially is not necessarily relevant from the point of view of aerosol formation.

Absolute Analysis

As stated in the introduction, for a method to be considered absolute, the following conditions should be met: (i) elimination of analytical matrix interferences, (ii) stabilization of calibration over time, and (iii) theoretical calculation of the calibration function based on fundamental parameters and actual measurement conditions [2]. The third condition, a theoretical expression for the LEI signal, will be discussed below.

The integrated LEI signal, S , in coulombs for our flame-LEI system with ETV (graphite furnace) sample introduction is given by:

$$S = \frac{96,485}{A_s} W_s \epsilon_v \epsilon_r \epsilon_a \epsilon_d \quad (36)$$

where W_s is the mass (g) of analyte in the sample, A_s is the

atomic weight of the analyte (g mol^{-1}), ϵ_v is the vaporization efficiency of the graphite furnace, ϵ_t is the transport efficiency between the furnace and the flame, ϵ_a is the atomization efficiency (or the free atom fraction, β) of the analyte in the flame, ϵ_p is the laser beam probing efficiency, and ϵ_d is the detection efficiency (efficiencies are all dimensionless). All of these efficiencies must be measured before considering the possibility of using this technique as an absolute method. Ideally these efficiencies should all be unity for absolute analysis, because, if they are not, there is a greater chance that they will vary from sample to sample. Also, the sensitivity of the method will be reduced if the efficiencies are not unity.

The transport efficiency, ϵ_t , describes how effectively the analyte vaporized in the furnace is transported to the flame. This value must be experimentally determined, as it is a characteristic of the experimental setup. The probing efficiency of the laser beams, ϵ_p , is a product of the spatial probing efficiency, ϵ_s , and the temporal probing efficiency, ϵ_t . The spatial probing efficiency describes what portion of the flame the laser beams encompass. If the lasers encompass the entire flame, then $\epsilon_s = 1$. The temporal probing efficiency is given by:

$$\epsilon_v = \frac{D_b f}{v} \quad (37)$$

where D_b is the diameter of the laser beam (cm), f is the frequency of the pulsed laser (Hz), and v is the flame velocity (cm s^{-1}). The vaporization efficiency of the furnace, ϵ_v , is assumed to be unity, provided the proper temperature and ramp times are chosen to control the graphite furnace. The atomization efficiency, ϵ_a , describes the portion of the sample that is actually present in the flame as free atoms capable of being ionized. This is a function of the analyte and the flame conditions and can be found in tables or experimentally determined [5,56,57].

The detection efficiency, ϵ_d , describes the charge collection by the electrode and the ionization efficiency induced by the laser in the flame. It is given by:

$$\epsilon_d = Y_i \epsilon_0 \quad (38)$$

where Y_i is the ionization yield and ϵ_0 describes the efficiency of charge collection. The actual signal detected in our case is the induced charge, Q_i , which is related to the total charge, Q_{tot} , by the equation:

$$Q_i = Q_{\text{tot}} \frac{\Delta V}{V} \quad (39)$$

where ΔV is the actual potential in the flame at the point of ionization and V is the potential applied to the electrode

[58]. The fraction $\Delta V/V$ describes the efficiency of charge collection, ϵ_D , in our case, is given by:

$$\epsilon_D = \frac{\Delta V}{V} \quad (40)$$

The ionization yield describes the fraction of atoms which become ionized in the flame due to the laser induced process. According to Omenetto et al. [59], when the second excitation transition reaches a Rydberg level from which collisional ionization occurs very rapidly, the ionization yield can be determined by measuring what is known as the fluorescence dip. This parameter describes the decrease in resonance fluorescence from the first excited level occurring when adding the second pumping process. This second excitation process depletes the atomic population of the first excited level such that they do not return to the ground state. The resonance fluorescence signal is always proportional to the number density of excited atoms in the first excited state [60]. As it has been shown from simple theoretical considerations [20,48,61], the ionization yield will approach unity when an optically saturating laser pulse has a duration that significantly exceeds the reciprocal of the effective ionization rate of the laser populated excited state. However, before using the fluorescence measurement to evaluate directly the ion yield, one must be sure that there

is no loss due to quenching collisions into a metastable level. In the absence of collisional quenching, the ionization yield can be calculated as:

$$Y_i = \frac{I_{21}(\lambda_1 \text{ only}) - I_{21}(\lambda_2 \text{ added})}{I_{21}(\lambda_1 \text{ only})} \quad (41)$$

where I_{21} is the signal intensity for the resonance fluorescence.

CHAPTER 4 REVIEW OF LASER ENHANCED IONIZATION

Analytical Performance of Flame-LEI

Limits of Detection and Sensitivities

The primary advantage LEI offers over other analytical methods is its very high sensitivity. With LEI, detection limits in the sub-ppb range have been achieved for many elements. There are several reasons for the high sensitivity of LEI: (i) electrical detection implies an almost 100% signal collection efficiency in a substantial part of the flame, (ii) high ionization efficiency in the interaction region of the flame, (iii) no background from scattered light, and (iv) molecular formation of the analyte atoms may be of less importance than in other methods since the sensitivity is high enough to compensate for this.

Table 1 lists over 200 experimentally measured limits of detection for flame-LEI of 34 elements. For the best cases, the measured limits of detection are within a factor of three of the theoretical detection limit. There are a number of elements which have detection limits in the sub-ppb range.

Table 1. LEI limits of detection [62]

El.	λ_1 (nm)	λ_2 (nm)	Laser	Flame	Time Con. (s)	LOD (ppb)	Ref
Ag	328.068	421.094	E	AA	-	0.075	63
Ag	328.068	546.549	Y	AA	-	0.3	64
Ag	328.068	547.155	Y	AA	-	0.4	65
Ag	328.068		Y	AA	-	2	65
Ag	328.068		F	AA	1.1	1	65
Al	265.248		E	AA	1	3	66
Al	266.039		E	AA	1	2	67
Al	308.215		F	AN	1	0.2	67
Al	309.271		F	AN	1	0.2	68
As	278.022		E	AA	1	3000	67
As	286.044		E	AA	1	50000	67
Au	242.795	479.266	Y	AA	1.4	1	68
Au	242.795		Y	AA	1.4	1000	69
Au	264.148		E	AA	1	4	67
Au	267.595		E	AA	1	1.2	67
Au	267.595	294	E	AA rod	-	0.02	69
Au	274.825		E	AA	1	200	67
Ba	270.263		E	AA	1	0.6	67
Ba	307.158		F	AA	1.1	0.2	66
Bi	302.464		E	AA	3	45	70
Bi	306.772		F	AA	1.1	2	66
Ca	272.165		E	AA	1	0.4	67
Ca	300.686		F	AA	1.1	0.1	66
Ca	422.673	468.527	N	AA	1	0.05	71
Ca	422.673	468.527	N	MA	1	0.5	72
Ca	422.673	585.745	Y	AA	1.5	0.03	72

Table 1 Continued

Ca	422.673	518.89	N	AA	1	0.02	72
Ca	422.673	518.89	N	MA	1	0.1	72
Ca	422.673	518.89	N	AA	1	0.02	73
Ca	422.673		Y	AA	1.5	15	73
Ca	422.673	518.885	N	HA	3	100	74
Ca	422.673		Kr cw	AA	0.3	1	75
Ca	422.673		N	HA	3	30000	75
Ca	422.673		N	AA	1	1	72
Ca	422.673		N	MA	1	10	72
Cd	228.802	466.235	Y	AA	1.4	0.1	69
Cd	228.802		Y	AA	1.4	100	69
Co	252.136	591.680	Y	AA	1.4	0.08	69
Co	252.136		Y	AA	1.4	10	69
Co	273.112		E	AA	1	50	67
Co	274.046		E	AA	1	25	67
Co	276.419		E	AA	1	6	67
Co	281.556		E	AA	1	7	67
Co	304.400		E	AA	3	6	71
Co	315.878	531.678	Y	AA	-	0.2	65
Co	315.878	534.339	Y	AA	-	0.2	65
Co	315.878		Y	AA	-	2	65
Co	321.915	515.405	Y	AA	-	0.3	65
Co	321.915		Y	AA	-	4	65
Cr	272.651		E	AA	1	0.9	67
Cr	278.070		E	AA	1	1.5	67
Cr	298.600		F	AA	15	2	76
Cr	301.492		E	AA	3	36	71
Cr	301.757		F	AA	15	2	77

Table 1 Continued

Cr	427.480	529.74	E	AA	-	0.5	77
Cs	455.531		N	PBA	-	0.004	78
Cs	455.531		N	PBA	1	0.004	79
Cs	455.531		N	PBA	0.1	0.1	80
Cs	455.500		N	AA	-	0.002	81
Cs	852.124		Diode	HA	1	0.25	82
Cu	276.637		E	AA	1	50	67
Cu	282.437		F	AA	15	100	77
Cu	282.437		E	AA	1	40	67
Cu	296.116		E	AA	1	600	67
Cu	324.754	453.078	E	AA rod	-	0.02	70
Cu	324.754	453.078	Y	AA	1.4	0.07	69
Cu	324.754		Y	AA	1.4	3	69
Cu	324.754		F	AA	15	100	18
Cu	324.754		Y	AA	1	2	83
Cu	324.754		Y	AA tc	1	2	84
Cu	510.600	453.078	N	HA	3	500	75
Eu	459.404	564.02	N	AA	0.1	4000	84
Fe	271.902		E	AA	1	0.1	67
Fe	273.358		E	AA	1	2	67
Fe	273.548		E	AA	1	3	67
Fe	274.698		E	AA	1	30	67
Fe	278.810		E	AA	1	1.5	67
Fe	281.329		E	AA	1	5	67
Fe	298.357		F	AA	15	4	77
Fe	302.064		E	AA	3	0.12	71
Fe	302.064		F	AA	15	2	77
Fe	318.490		Y	AA	-	100	65

Table 1 Continued

Fe	319.166		Y	AA	-	4	65
Fe	319.323		Y	AA	-	3	65
Fe	321.440		Y	AA	-	200	65
Fe	364.784	538.337	N	HA	3	100	75
Fe	364.784		N	HA	3	2000	75
Ga	265.987		E	AA	1	0.1	67
Ga	271.965		E	AA	1	0.04	71
Ga	287.424		F	AA	15	0.07	77
Ga	287.424		E	AA	1	0.06	67
Ga	294.364		E	AA	3	0.06	71
Ga	294.364		F	AA	15	0.1	77
Ga	417.200		Kr cw	AA	0.3	60	76
In	271.026		E	AA	1	0.001	67
In	271.394		E	AA	1	0.008	67
In	275.388		E	AA	1	0.005	67
In	293.263		E	AA	1	0.03	67
In	303.936	532	Y	AA	75	0.0004	85
In	303.936	786.4	Y	AA	-	0.03	4
In	303.936		F	AA	1.1	0.006	66
In	303.936		F	AA tc	1	0.1	84
In	303.936		F	AA	1	0.02	84
In	303.936		Y	AA tc	1	0.1	86
In	303.936		Y	AA	1	0.02	87
In	303.936		F	AA	15	0.008	77
In	303.936		Y	AA	-	0.007	82
In	303.936		E	AA	3	0.03	71
In	410.176		Kr cw	AA	0.3	20	76
In	451.131	571.0	E	AA rod	-	0.0004	87

Table 1 Continued

In	451.131	501.8	N	HA	3	0.6	75
In	451.131	501.8	N	AA	-	0.007	82
In	451.131	502.3	N	AA	-	0.03	82
In	451.131	525.4	N	AA	-	0.003	82
In	451.131	526.3	Y	AA	-	0.01	82
In	451.131	571.0	N	AA	-	0.001	82
In	451.131	572.8	N	AA	-	0.03	88
In	451.131	572.8	N	AA	-	0.003	82
In	451.131		Kr cw	AA	0.3	0.1	76
In	451.131		N	HA	3	100	75
Ir	266.479	562.004 + 642.0	E	AA	1	0.3	89
K	294.268		F	AA	15	1	77
K	296.321		E	AA	1	1.5	67
K	404.414		N	PBA	-	0.1	79
K	580.200		E	AA	-	0.1	90
K	766.490		Kr cw	HA	0.3	0.1	76
Li	274.119		E	AA	1	0.005	67
Li	460.286		Kr cw	AA	0.3	20	76
Li	610.362		F	AA	1.1	0.01	66
Li	639.146	639.146	F	AA	1.1	0.4	66
Li	670.784	460.286	E	AA	-	0.0003	64
Li	670.784	610.362	N	HA	3	0.04	75
Li	670.784	610.36	Y	AA	0.1	0.03	81
Li	670.784		F	AA	1.1	0.001	66
Li	670.784		N	HA	3	4	75
Mg	285.213	435.2	Y	AA	-	0.002	4
Mg	285.213	470.3	N	AA	0.1	0.4	91
Mg	285.213		F	AA	15	0.1	18

Table 1 Continued

Mg	285.213		E	AA	3	0.005	71
Mn	279.482		E	AA	1	0.04	67
Mn	279.482	521.482	Y	AA	1	0.02	92
Mn	279.482		F	AA	15	0.3	18
Mn	279.827		E	AA	1	0.05	67
Mn	279.984		F	AA	15	5	18
Mn	280.106		E	AA	1	0.08	67
Mn	292.557		E	AA	1	3	67
Mn	292.557		E	AA	3	3	71
Mn	403.076	602.180	N	HA	3	5	75
Mn	403.076		N	HA	3	30	75
Mo	267.985		F	AN	1	30	68
Mo	306.428		F	AN	1	400	68
Mo	307.437		F	AN	1	500	68
Mo	308.562		F	AN	1	500	68
Mo	311.212		F	AN	1	900	68
Mo	313.259		F	AN	1	70	68
Mo	315.816		F	AN	1	70	68
Mo	317.035		F	AN	1	20	68
Mo	319.397		F	AN	1	10	68
Mo	320.883		F	AN	1	50	68
Na	268.037		E	AA	1	0.1	67
Na	268.046		E	AA	1	0.1	67
Na	285.281		E	AA	3	0.0015	71
Na	285.301		F	AA	15	0.05	18
Na	540	540	Y	PBA	-	70	79
Na	550	550	Y	PBA	-	3	79
Na	578.732	578.732	E	AA	-	0.001	93

Table 1 Continued

Na	578.732	578.732	Y	PBA	-	0.9	79
Na	588.995	568.266	E	AA	-	0.003	64
Na	588.995	568.821	N	HA	3	0.04	75
Na	588.995	568.821	Y	AA	-	0.012	94
Na	588.995	568.821	Y	PBA	-	0.002	79
Na	588.995	568.821	N	AA	-	0.0006	82
Na	588.995	616.075	Y	PBA	-	0.01	79
Na	588.995		Kr cw	AA	0.3	0.03	76
Na	588.995		N	HA	3	6	75
Na	588.995		E AL	HA	10	0.3	95
Na	588.995		E	AA	-	0.02	94
Na	588.995		F	AA	-	0.01	96
Na	588.995		F	AA	-	20	97
Na	588.995		Y	HA	1	0.8	98
Na	588.995		Y	AA	1	0.6	99
Na	589.592	568.263	N	AA	-	0.001	82
Na	589.592	568.26	N	AA	0.1	0.005	92
Na	589.000	449	E	AA rod	-	0.0002	70
Na	588.995		F	AA	15	0.1	18
Ni	269.649		E	AA	1	24	67
Ni	279.865		E	AA	1	0.4	67
Ni	282.129		E	AA	1	0.3	67
Ni	300.249		F	AA	1.1	7	66
Ni	300.249		F	AA	15	8	77
Ni	300.249	576.755	Y	AA	1.4	0.08	69
Ni	300.249		Y	AA	1.4	8	69
Ni	301.200		E	AA	3	1.5	71
Ni	324.846		Y	AA	-	2	65

Table 1 Continued

Pb	280.199		E	AA	1	0.4	67
Pb	280.199		F	AA	15	0.6	18
Pb	282.320		E	AA	1	0.5	67
Pb	282.320	600.193 + 1064	Y	AA	75	0.0007	86
Pb	282.320		F	AA	15	3	18
Pb	283.306	600.193	Y	AA	1.4	0.09	69
Pb	283.306	600.193	E	AA	-	0.3	64
Pb	283.306		Y	AA	1.4	3	69
Pb	283.306		E	AA	1	0.2	67
Pb	287.331		E	AA	3	3	71
Pb	287.331		E	AA	1	0.6	67
Rb	420.185		Kr cw	HA	0.3	0.7	76
Rb	420.185		N	PBA	-	0.1	79
Rb	420.185		N	AA	1	0.0006	74
Rb	780.023		K	HA	0.3	0.09	76
Rb	780.023		Diode	HA	1	0.3	83
Sb	276.995		E	AA	1	90	67
Sb	287.792		E	AA	1	50	67
Si	288.158		F	AN	1	40	68
Sn	266.124		E	AA	1	30	67
Sn	270.651		E	AA	1	8	67
Sn	270.651		F	AN	1	2	68
Sn	283.999	597.028	Y	HA	1.4	0.3	69
Sn	283.999		Y	HA	1.4	8	69
Sn	283.999		E	AA	1	2	67
Sn	283.999		F	AN	1	0.4	68
Sn	283.999		F	AA	15	6	77
Sn	286.333		F	AN	1	2	68

Table 1 Continued

Sn	286.333		F	AA	15	10	77
Sn	286.333		E	AA	3	20	71
Sn	286.333		E	AA	1	3	67
Sn	300.914		F	AN	1	10	68
Sn	303.412		F	AN	1	6	68
Sn	317.505		F	AN	1	3	68
Sn	326.234		F	AN	1	2	68
Sr	293.183		E	AA	1	0.01	67
Sr	459.513		E	AA	-	15	99
Sr	460.733		K	AA	0.3	0.4	76
Sr	460.733		Y	HA	1	3	99
Sr	460.733		Y	AA	1	1	99
Sr	460.733	554.336	E	AA	-	0.3	100
Ti	294.200		F	AN	1	10	68
Ti	294.826		F	AN	1	8	68
Ti	295.613		F	AN	1	6	68
Ti	300.087		F	AN	1	20	68
Ti	318.645		F	AN	1	1	68
Ti	319.199		F	AN	1	1	68
Ti	319.992		F	AN	1	1	68
Ti	331.442		F	AN	1	3	68
Ti	334.188		F	AN	1	2	68
Ti	335.469		F	AN	1	3	68
Ti	337.145		F	AN	1	4	68
Tl	276.787	377.572	E	AA	1	0.008	100
Tl	276.787		E	AA	10	0.02	101
Tl	276.787		E	AA	1	0.006	67
Tl	291.832		E	AA	3	0.02	71

Table 1 Continued

Tl	291.832		E	AA	1	0.008	67
Tl	291.832		F	AA	15	0.09	77
Tl	377.572		E AL	HA	10	3	96
Tl	377.572	655.6	Y	AA	-	0.01	4
V	292.362		F	AN	1	20	68
V	305.633		F	AN	1	6	68
V	306.046		F	AN	1	4	68
V	306.638		F	AN	1	3	68
V	318.398		F	AN	1	0.9	68
V	318.540		F	AN	1	0.9	68
W	283.138		E	AA	1	300	67
Yb	267.198		E	AA	1	1.7	67
Yb	555.647	581.2	Y	AA	-	0.1	82
Zn	213.856	396.545	Y	AA	1	1	101
Zn	213.856		Y	AA	1	3	102
Zn	307.590	472.216	Y	AA	1	15	102

E=excimer pumped dye laser, E AL=excimer pumped atomic line laser, F=flashlamp pumped dye laser, Kr cw=krypton ion pumped cw dye laser, N=nitrogen pumped dye laser, Y=Nd:YAG pumped dye laser, AA=acetylene/air, AN=acetylene/nitrous oxide, HA=hydrogen/air, MA=methane/air, PBA=propane/butane/air, rod=graphite rod in flame, tc=total consumption burner.

The lowest detection limits are obtained for elements with good atomization in the flame and low ionization potentials such as Li, Na, In, and Tl. This demonstrates that collisional ionization is very efficient from excited states close to the ionization limit. The low limits of detection obtained for one-step LEI for some of the other elements with comparatively higher ionization limits, such as Mg and Cd, suggest that alternative ionizing routes may exist.

Unfortunately, in many cases, the measured detection limits are much worse than the theoretical values [63]. This is due to a variety of reasons: poor atomization fractions, high contamination levels in blanks, radio frequency interference, low repetition rate lasers, high thermal ionization fractions, and the use of non-optimum excitation wavelengths.

Noise and Interferences

LEI detection limits are usually limited by noise or spectral interferences during the measurement. Sources of noise can be separated into two categories: multiplicative and additive. Multiplicative noises in LEI arise from the fluctuations in atomic population, fluctuations in the ionization yield, and fluctuations in the detection efficiency. Sources of additive noise include fluctuations in

the thermal background ionization, fluctuations in the laser-induced background ionization, and electronic noise.

Fluctuations of the atomic population within the irradiated volume of the flame result from fluctuations in the nebulization rate and in the flame gas flows. Fluctuations in the ionization yield are a result of changes in the laser output properties, such as the pulse-to-pulse power variation in the dye laser output. A 4% RSD is typical but may be worse in some circumstances. This is further complicated by the variation in laser power across the beam profile, where the power is higher at the center of the beam than at the edges. However, this problem may be minimized by saturation of the atomic transitions. Fluctuations in the temperature of the atom reservoir also contribute to fluctuations in the ionization yield.

Fluctuations in the detection efficiency can result from fluctuations in the high voltage power source for the electrode, variations in the flame composition, and spatial fluctuations of the laser beam.

As the concentration of the analyte decreases, multiplicative noise decreases; however, additive noise remains even in the absence of analyte. Therefore, it is usually the additive noises that ultimately limit the detection capability of the system.

Fluctuations in thermal ionization additive noise are a

result of fluctuations in the number of natural flame ions and sample matrix ions. These fluctuations may be a result of the flame flow fluctuations and nebulizer-induced noise.

Electronic additive noise results from the noise of the various electronic components used to measure the LEI current. Of the detection electronics used, the current preamplifier is the noisiest. Another source of electronic noise that may be significant is radio frequency (rf) noise. The LEI electrodes and preamplifier seem to act as an excellent antenna and detector for rf noise, so care should be taken to shield and ground the LEI instrumentation.

Random fluctuations in the laser-induced background may result from laser-induced ionization of spectral interferences. Spectral interferences can be caused by any matrix element but are most often a result of easily ionized elements. Also, spectral interferences may result from the overlapping of atomic lines but are usually a result of an overlap between the analyte line and some broadband spectral feature of a matrix component.

Line overlaps are rare and are easy to eliminate when two-step LEI is used. However, one disadvantage of using two-step excitation is that interference could occur at one or both wavelengths.

Overlaps between analyte lines and broadband spectral features of matrix constituents are, again, much more likely

to be encountered than direct spectral line overlaps. Such interferences include line wings, molecular bands, and thermionic ionization of particles. The wings of atomic lines are easily observed in laser spectroscopy, including LEI. An example of this is the line wing interference from Na on the determination of Ni by two-step (300.249 nm and 561.479 nm) LEI [63]. The most common molecular band interference encountered in LEI is due to LEI of CaOH [102]. The prevalence of Ca in many sample matrices, the incomplete dissociation of CaOH in the air/acetylene flame, the rather low ionization potential of CaOH (5.7 eV), the broad spectrum from green to red wavelengths, and the location of many second-step LEI stepwise excitation lines in this wavelength range combine to make this a common problem. Laser-induced particle ionization, may occur when a fuel-rich flame is being used or when certain organic solvents are aspirated. The mechanism for this is thought to be thermionic in nature [103]. It may be possible to correct for these by scanning the laser wavelength across the analyte line and performing the appropriate background correction [104]. Wavelength modulation has also been used to deal with these interferences [105].

Applications of LEI to Real Samples

LEI is one of the most sensitive analytical methods for trace element analysis. Unfortunately, LEI has found limited applications to real samples because of its susceptibility to easily ionized matrix elements. The inherent ease of collecting and sensing ions that contribute to the simplicity of the LEI detection scheme also makes it vulnerable to these easily ionizable elements (EIEs) [106]. So, although the laser affords a good amount of selectivity, it cannot compensate for an indiscriminating detector.

Sample dilution was the first solution to matrix interferences. It was often possible to dilute sufficiently the sample matrix and still detect the analyte because of the high sensitivity afforded by LEI. The use of an immersed electrode also helped to reduce the loss of LEI signal due to ion collection interferences [107], but did not reduce the dc background current from EIEs.

Today, approaches to analyze real samples by LEI can be categorized as involving interferant removal or those without interferant removal.

Determinations Without Interferant Removal

LEI is particularly amenable to samples of high purity with small amounts of EIEs. In these cases, little accommodation for interferences is necessary. Alloy samples are particularly well suited to LEI because they typically

contain low levels of sodium and potassium. The determination of indium in nickel-based, high-temperature alloys [22] is an early example of application of LEI spectrometry to a difficult analytical problem. An acetylene/air flame on a slot burner and plate electrodes produced satisfactory results because of the low levels of EIEs. Similar samples usually require a time-consuming extraction before conventional furnace atomic absorption analysis, in contrast to LEI where the alloy samples were successfully analyzed without sample preparation. The results were also in close agreement with values obtained with furnace atomic absorption.

Lowering the temperature of the atom reservoir is also a potential solution for analytes with low atomization temperatures such as cesium. Using a solid stainless-steel rod immersed in a low temperature propane/butane/air flame, researchers were able to determine accurately low concentrations (ng/mL) of cesium in tap water samples by LEI even with tens of mg/mL of sodium, potassium, and calcium present [80].

Natural water samples are also ideal for LEI. The concentrations of several elements at pg/mL levels were validated in a simulated rainwater Standard Reference Material (SRM 2694) by researchers at NBS (now NIST) using LEI spectroscopy [73]. LEI was one of the unrelated methods used to certify the concentration of the standards at NBS. Some

spectral interferences due to excitation in the wings of nearby peaks were corrected by standardization using matrix matched standards.

Two-step excitation has been used to determine zinc in SRM 1643a, trace elements in water, in the presence of a background interference [102]. The experimental value for zinc was slightly high, but no attempt was made to remove potential interferences beyond using an immersed electrode and sample dilution. It was felt that matrix matching of the standards would have improved the accuracy of the measurement.

As part of an environmental monitoring program, lead was determined in unpolluted waters from mountainous regions and compared with results for natural waters impacted by industrial development [108]. Many spectroscopic techniques do not have adequate sensitivity to determine species which are naturally present at very low background levels. These pristine waters presented little difficulty because of the very low levels of impurities. In the case of water impacted by industry, the concentrations of calcium, potassium, sodium, and magnesium impurities were 4-5 orders of magnitude larger than the lead concentrations and produced broad background signals. It was found that CaOH molecules were responsible for the interference at both excitation wavelengths but, by tuning off the resonance lines, it was possible to use background subtraction successfully.

Several elements have been determined in rock samples by LEI spectrometry [109]. Most of the other analytical methods require the use of complicated procedures prior to analysis unless the sample is preconcentrated or interferences are removed. However, for LEI the dissolved samples were aspirated into a propane/butane/air flame with an immersed electrode used for detection. Although a broad ionization background was found (due to CaOH), by reduction of the laser powers used, good agreement with certified values was obtained using aqueous standards. Detection limits of 0.002, 0.001, and 0.5 $\mu\text{g/g}$ were obtained for cesium, lithium and rubidium, respectively.

LEI spectrometry has also been demonstrated as a viable approach for detecting dopants and impurities in acid-dissolved bulk gallium arsenide [110]. By using a two-step excitation scheme, background subtraction was possible. Trace amounts of chromium, iron, nickel, indium, manganese, and cobalt were detected. Two-step LEI has also been used to determine sodium in semiconductor silicon [111].

LEI has been used for determination of trace amounts of nickel in petroleum products because nickel poisons the catalysts used in petroleum processing [112]. Samples of both heavy-oil flash distillate and an oil-based SRM were diluted with a xylene/*n*-butanol solvent mixture and aspirated into an

air/acetylene flame. Nickel determination in the SRM was in good agreement with the NIST certified value. Because of the high sensitivity of LEI, it was possible to dilute the samples considerably which nearly eliminated the need for matrix matching of the standards.

Determination of indium in a CdHgTe alloy was accomplished in both liquid solutions and solid samples without sample preparation [70,113]. Electrothermal atomization was coupled with LEI spectrometry by inserting a resistively heated graphite rod in a premixed flame of a slot burner. Propane/butane/air and acetylene/air flames were used. No matrix interference was found for the samples and aqueous standards were used for calibration. A good correlation between results for liquid and solid samples indicated analytical accuracy and an absence of analyte losses for solid sampling.

Determinations With Interferant Removal

Preionization has been used for removal of spectral interferences and is described in more detail elsewhere [114]. Magnesium was chosen as the analyte since it is very susceptible to interference from sodium (atomic wing absorption). Several preionization schemes were investigated using up to three photons of different energies. Up to an 83% sodium depletion in the flame was achieved. A probe laser

then interrogated the preionized "hole" with 285 nm photons to enhance thermal ionization of the analyte. Although satisfactory results were achieved, the technique will probably not be widely utilized because of the cost involved for the two separate laser systems, the complexity in timing the arrival of the ionization laser beam(s) and the probe laser beam, and because signal collection interferences are related to the bulk flame environment and are not relieved by laser preionization.

Chekalin and others determined copper and sodium in concentrated orthophosphoric acid using their rod-flame system [70,114]. The sodium interferant was removed by selective volatilization from the dried sample at 1000°C. When the temperature was raised to 2000°C, the copper signal could be detected in the absence of noise. Detection limits were determined by the purity of the rod material.

The determination of lead in a blood matrix has also been reported [115]. A graphite furnace, used for sample vaporization, was coupled with an acetylene/air miniature flame for the analysis. With only a 21:1 dilution using ultra pure water and temperature programming of the graphite furnace, a detection limit of 0.089 ng/mL (890 fg absolute) for lead in whole blood was obtained.

Solvent extraction has been shown to be effective for the determination of trace amounts of manganese using a single-

step excitation scheme [116]. Manganese was complexed in water with sodium diethyldithiocarbamate and extracted into diisobutyl ketone. The extraction resulted in a 10-fold increase in the concentration of the manganese as well as interferant removal. This method was successfully applied to the analysis of ng/mL of manganese in groundwater, river and lake waters, seawater, tap water, and wastewater.

An extraction also made the determination of 0.001% calcium in aluminum alloys possible [72]. The separation was based on the different solubilities of calcium and aluminum chlorides in methanol. The detection limit was determined by the purity of the methanol used.

Chromatography using a chelating resin to separate the interfering elements from the analyte was used to determine trace amounts of copper in a sulfate plating solution and seawater [65]. The removal of EIEs was accomplished using Chelex 100 [117]. In this process, transition and heavy metals were chelated in the 5.2-5.6 pH range while ammonium acetate was used to selectively elute the alkali and alkaline earth metals by ion exchange. In the final step, the trace metals were eluted with nitric acid and introduced into a burner for LEI spectrometry. A microsampling cup coupled to a premix burner (acetylene/air) permitted absolute determinations of copper as low as 50 pg. Silver, cobalt, iron, and nickel were also detected.

Turk and Kingston have combined automated chelation chromatography with computer-controlled LEI spectrometry to determine a large number of elements in a wide range of NIST SRMs [105]. Chelex 100 resin was used for the separation which was automated with a laboratory robot after preliminary work. The elements determined and the reference materials analyzed included the following: Cd, Co, Cu, Mn, Ni, and Pb in Trace Elements in Water (SRM 1643b), Mn and Ni in Inorganic Constituents in Bovine Serum (SRM 1598), Ni and Pb in Buffalo River Sediment (SRM 2704), Cu, Mn, and Ni in Total Diet (SRM 1548), and Mn and Ni in Apple Leaves (SRM 1515⁶) and in Peach Leaves (SRM 1547). Concentrations determined ranged from the mg/g to the ng/g range while precisions were in the range from 0.8% to 36% RSD. It was hoped that this impressive display of technology would go a long way towards establishing LEI spectrometry as a practical analytical method.

Alkyltins in sediment were determined by ion-exchange chromatography coupled with LEI detection [106,118]. Tributyltin was extracted into 1-butanol and two-step (284.0 nm and 603.8 nm) LEI was performed in an acetylene/air flame. The detection limit determined with the LEI detector was 3 ng/mL tin as tributyltin or 60 pg of tin.

The coupling of liquid chromatography with LEI has also been reported for the measurement of organolead species [119]. Two Nd:YAG pumped dye lasers were used to optically excite

lead at 283.31 nm and 600.19 nm. A reversed phase LC column was attached to the LEI acetylene/air flame. A detection limit of 0.9 ng/mL (20 pg Pb for 20 μ L injection) for tetraethyllead was calculated. Oyster tissue samples (SRM 1566a) were analyzed. Trace levels of trimethyllead were observed in the Oyster tissue, but concentrations varied among the samples tested. This seemed to indicate that the extraction and digestion procedures used were inadequate.

The use of flow injection analysis to reduce the electrical interference from a sodium matrix for LEI has been reported [120]. A frequency doubled Nd:YAG laser provided optical excitation at 325.62 nm for LEI of indium. A typical slot burner and nebulizer were used. A flow injection apparatus was used to handle the solution prior to the nebulizer. The standard addition method was also used with this system to recover the original In concentration. This combination of flow injection analysis and LEI was capable of detecting In in a Na matrix of over 40 ppm, which is about 20-fold more than the conventional LEI apparatus could tolerate alone. This system also exhibited a larger linear dynamic range for In, which was extended to 30 ppm with a mixture of 8 ppm Na matrix, up from 5 ppm for the conventional LEI system.

Although the future for applications of LEI spectrometry

looks good, for LEI to become more widespread will require continued evolution of hardware and software to accommodate routine analysis by LEI. Coupling of LEI to other techniques has also enhanced its ability to handle real samples. It has been suggested that perhaps a multi-capability "laser spectrometer" may be considered more promising for commercial LEI instrumentation [121].

Hybrid Techniques and Non-Flame Atom Reservoirs

Although the flame is the most commonly used atom reservoir for trace element analysis by LEI, the flame atomizer alone has some serious drawbacks for trace element analysis: (i) dilution of sample vapors by flame gas combustion products, (ii) limited range of temperatures used, (iii) a small (0.1-0.15) sample utilization factor (fraction of the sample that reaches the flame), (iv) the impossibility of separating the processes of sample evaporation and atomization, (v) problems associated with handling microvolumes of liquids and solid samples, and (vi) combustion products of flames may hinder some of the spectral regions for successful implementation of LEI [122]. These limitations have prompted consideration for hybrid techniques and alternate atom reservoirs for LEI spectrometry.

Electrothermal Vaporizers

The first attempts to use a graphite furnace for LEI determinations of elements failed [108]. Later, Gonchakov et al. reported the successful application of electrothermal atomization for determination of small amounts of sodium using a three-step ionization scheme [123]. A graphite cup in an argon atmosphere was used as an atomizer and a tungsten loop, positioned 2 cm above the graphite cup, was used as an electrode. A detection limit of 1 fg was calculated for Na.

Torres used a Varian-Techtron CRA-90 electrothermal tube atomizer for LEI spectrometry [124]. The electrode and graphite tube were positioned end-to-end on the same axis with the laser beams passing through the graphite tube. A detection limit of 5 pg was achieved for Cs. However, other metals could not be determined because of thermionic emission at higher temperatures and also because of arcing between the electrode and graphite tube.

Graphite furnace-LEI was also used to determine the presence of sodium and indium at the fg level [82]. A tungsten wire was placed axially inside the graphite tube. The LEI signal was found to be 10-100 times larger than in a flame, but the reproducibility was poor. Arcing between the electrode and graphite tube also occurred when the temperature was increased.

The most detailed investigations of LEI in the graphite

furnace were made by Magnusson and others [125,126,127]. However, they were faced with the same problems encountered in the previously mentioned studies. Thermionic emission from the graphite tube and electrode made it impossible to detect elements which atomized at high temperatures. Although the sampling efficiency (fraction of sample introduced that reaches the probing area) was 2-3 orders of magnitude higher than that in a flame, the limits of detection were on the same order of magnitude. This was partially due to the lower rate of collisional ionization in the argon atmosphere of the graphite furnace.

A T-shaped furnace was suggested by Magnusson and demonstrated by Sjöström to solve the thermionic emission problem by spatially separating the regions of atomization and detection [128]. A flow of argon was used to transport the atoms to an external cavity adjacent to the tube, in which laser excitation and LEI detection were performed. Detection limits in the pg range were obtained for manganese and strontium. However, this system had some drawbacks. As a result of the temperature gradient between the center of the graphite tube and the detection region, relatively few of the atoms in the sample actually reached the detection region.

The use of modern furnace technology with probe atomization for LEI has been described by Butcher et al.

[129]. In this system, a graphite probe was used for both sample introduction and as the high-voltage electrode (-50 V). The sample was vaporized off of the probe into an already isothermal, furnace environment, which reduced the matrix interferences mentioned above and prevented atom condensation onto the probe. For elements such as Tl, In and Li, detection limits were between 0.7 and 2 pg. For Pb, Mg, and Fe, detection limits were between 10 and 60 pg. The linear dynamic range was between 3 and 4 orders of magnitude with a precision between 12 and 16% for aqueous solutions. Sodium matrix effects were also investigated and found to suppress the LEI signal in the same manner as in the flame, so similar difficulties would be encountered in the graphite furnace with complex matrices as in the flame.

A novel design for a graphite furnace atomizer-ionizer was examined by Chekalin and Vlasov [70]. Their outer electrode design along with careful selection of the applied electrode voltage suppressed interference from thermionic emission of the heated graphite tube. Detection limits of 0.08 pg/mL for In and 100 pg/mL for Yb were obtained. This system seems very promising for analysis of high purity materials.

Hybrid Combinations of Flame and Electrothermal Vaporizers

Hybrid combinations of the flame and electrothermal

vaporizer were developed in order to alleviate the problems associated with LEI in the graphite furnace alone, which were mentioned above. The combination of flame and electrothermal vaporizer/atomizer was first proposed by Chaplygin et al. [130]. Their system consisted of a specially designed cylindrical burner which contained an electrically heated wire loop or filament in the central channel. An argon flow up the central channel carried the sample vaporized off the wire loop up into the flame. This design helped to minimize the sample matrix by using small injection volumes and by temperature programming of the sample vaporization loop. Detection in the flame eliminated interference from thermionic emission from heating of the sample loop and also maximized the LEI signal because the flame region irradiated by the laser beams was located much higher than the combustion zone. A detection limit of 0.5 pg for Cs with reproducibility of 5-6% was obtained.

Miyazaki and Tao have reported the use of a commercial electrothermal vaporizer as a sample introduction system for LEI spectrometry [131]. The commercial electrothermal vaporizer (ETV) used (Seiko Instruments Inc., Tokyo) consisted of a tungsten boat and a glass chamber. A Nd:YAG pumped dye laser provided optical excitation at 276.79 nm and 291.83 nm for one-step LEI of thallium. EIEs were found to interfere at

a 10-fold excess or more. Tl was extracted into 2,6-dimethyl-4-heptanone (DIBK) with ammonium tetramethylene dithiocarbamate (APDC) and hexamethylenearmonium hexamethylenedithiocarbamate (HMAHMD) at pH 6 to remove EIE interferences. Detection limits of 0.043 ng/mL (276.79 nm) for Tl with the extraction and 0.11 ng/mL (291.83 nm) for Tl without the extraction were obtained. This system was then applied to and found to be useful for the analysis of different types of natural water samples.

In order to acquire the advantages of both graphite furnace vaporization and flame ionization detection while maintaining independent control of each process, Smith et al. have reported the coupling of a graphite furnace with a miniature acetylene/air flame for LEI detection [132]. The graphite furnace was used to vaporize samples which were transported to the flame by a flow of argon gas. Two Nd:YAG pumped dye lasers provided optical excitation at 285.2 and 435.2 nm for Mg, 377.6 and 655.6 nm for Tl, and 303.9 and 786.4 nm for In. Limits of detection of 0.0017 ng/mL (17 fg absolute) for Mg, 0.012 ng/mL (118 fg absolute) for Tl, and 0.026 ng/mL (260 fg absolute) for In were obtained.

Riter et al. have reported the use of a modification of the above system for trace element analysis [133]. A commercially available graphite furnace (Finnigan MAT/SOLA,

Bremen, Germany) was used to vaporize samples which were subsequently transported to a redesigned miniature burner, which supported an acetylene/air flame, by a flow of argon gas. Two XeCl excimer pumped dye lasers were used to provide optical excitation at 285.213 and 435.191 nm for the analysis of Mg. A complete determination of the instrumental characteristics of the above system for the analysis of Mg was performed. A blank-limited detection limit of 2 ng/mL (20 pg absolute) was obtained for Mg. A detection limit of 590 fg/mL (5.9 fg absolute) was calculated in the absence of a blank signal and a reduction of the radio frequency noise.

Riter et al. also evaluated the above system for the determination of trace Pb concentrations in whole blood [116]. Optical excitation at 283.3 and 509.0 nm was provided by two XeCl excimer pumped dye lasers. Bovine blood samples from the Centers for Disease Control (CDC) and NIST (SRM 955a) were analyzed. With temperature programming of the graphite furnace, there appeared to be no interference from the blood matrix, and, instead, the matrix appeared to produce a carrier effect, increasing the transfer efficiency between the furnace and the flame over that for aqueous standards. The authors concluded that there was sufficient matrix removal from temperature programming of the graphite furnace and that the matrix remaining acted as a carrier. A detection limit of

0.089 ng/mL (890 fg absolute) was calculated for Pb in whole blood. This technique appears to have great promise for the analysis of samples with complex matrices.

Marunkov reported the first LEI experiments with sample vapors being introduced into a flame by an electrically heated graphite rod and by diffusion through the wall of an electrically heated closed graphite tube [134]. Detailed experiments were not carried out, but results appeared to be promising.

A hybrid "rod-flame" arrangement was proposed by Chekalin et al. to combine the advantages of flame and electrothermal atomizers [70,88,114,135]. In their system, the sample is evaporated by an electrically heated graphite rod into the flame where the analyte is atomized, laser excited, ionized, and then detected. Advantages of this system included an increase of the sample utilization factor (fraction of the sample introduced that reaches the probing region), the analysis of microsamples, and the direct analysis of solid samples. However, the researchers encountered problems with nonselective background ionization from the compounds evaporating from the heated graphite rod and impurities in the graphite were contributing to a blank signal. Good detection limits were obtained for many elements including Au (2 pg/mL), Co (100 pg/mL), Cr (20 pg/mL), Cu (2 pg/mL), In (0.04 pg/mL),

Mn (30 pg/mL), Na (0.02 pg/mL), and Ni (8 pg/mL). The analysis of high-purity substances, such as Na and Cu in orthophosphoric acid, Cu in germanium, In in Cd-Hg-Te alloy, and Cr, Co, Mn, and Ni in fluorine-containing materials for optical fibers, was also demonstrated. Detection limits ranged from 0.1 to 7,000 ng/g for the different elements.

LEI in the Inductively Coupled Plasma

The first measurements of LEI in the ICP were made by Turk and Watters [136]. Resonant LEI was detected for Fe, Mn, Na, and Cu, however, the population of free atoms was too small so the sensitivity was very poor. Turk et al. used a power modulated ICP to reduce the rf interference from the plasma [137]. With their approach, detection limits of 80 ng/mL for Fe and 20 ng/mL for Ga were achieved which are still poorer than for the flame.

Ng et al. reported significant improvements in the detection limits by using an extended-torch ICP, modifying the torch and electrode designs, and using a continuous wave laser [138]. The smaller electrode dimensions and smaller separation between electrodes used by Ng et al. probably accounted for the 2 orders of improvement in the detection limit over Turk and Watters. Limits of detection ranged from 30 ng/mL for Ca to 810 ng/mL for Sr. Although these are an improvement, they are still worse than the detection limits

for flame and furnace LEI.

The coupling of ICP and flame LEI with mass spectrometric detection has been reported by Turk and others [139,140,141]. With a modified commercial ICP-mass spectrometer (ICP-MS), Sr was examined employing laser-induced ionization (460.733 nm and 308 nm). An enhancement of only 11% in the Sr^+ ion signal was observed with the addition of laser excitation. The flame was found to offer a much better environment for laser-induced ionization or LEI than the ICP. A hydrogen/air flame was used for Na, K, and Fe while an acetylene/air flame was used for Ca. A 350 times increase in the signal was observed for Na^+ with the addition of two-step optical excitation (589.0 nm and 498.3 nm). A detection limit of 0.05 ng/mL for Na was calculated. Detection limits of 0.14 ng/mL for K (766.5 nm and 580.2 nm), 35 ng/mL for Fe (302.1 nm), and 61 ng/mL for Ca (422.7 nm and 585.7 nm) were obtained. The poor detection limit for iron was believed to be due to one-step excitation, and the detection limit for Ca was thought to be due to the poor atomization efficiency of Ca in the acetylene/air flame.

Other Methods and Reservoirs

Gorbatenko et al. have reported the use of a Nd:YAG laser as a laser microprobe solid sampling device for flame LEI [142]. The sample was positioned at the edge of the burner head to allow for the direct transport of the sample vapors to

the combustion zone. Lithium was chosen as the analyte and was ablated from an aluminum alloy sample. Optical excitation was provided by two Nd:YAG pumped dye lasers at 670.8 nm and 610.4 nm. It was found that the atomization efficiency was determined by flame temperature and composition regardless of how the sample was introduced into the flame. It was also found that this technique allowed for the study of the distribution of Li impurities over the surface of a solid sample with a spatial resolution of about 100 μm . A detection limit of around 30 $\mu\text{g/g}$ for Li in solid samples was achieved with a very short (≤ 20 s) analysis time.

Churchwell et al. have investigated the atmospheric-pressure microarc atomizer as an atom reservoir for LEI [143]. Microvolumes of analyte solution were deposited on the tip of the tungsten cathode loop and dried with a heat gun. LEI measurements were performed directly in the plasma above the microarc discharge. A detection limit of 3 ng for Na was estimated. Preliminary results indicate that the helium-microarc-induced plasma may be feasible for LEI spectrometry but further studies are needed.

From the above examples, it can be seen that alternate atom reservoirs and hybrid techniques have been used with varying degrees of success for LEI spectrometry. The flame still appears to be the optimal atom reservoir for LEI.

However, the hybrid techniques appear to be the most promising of those discussed, especially for dealing with the matrix interferences from real samples. Further research on their application to samples with complex matrices is warranted.

CHAPTER 5 EXPERIMENTAL

LEI

A block diagram of the experimental setup used for graphite furnace-LEI is shown in Figure 6. An excimer laser (Model LPX-240i, Lambda Physik, Acton, MA), operated with XeCl, was used to pump two dye lasers (Model Scanmate 1, Lambda Physik, Acton, MA). The output of the dye lasers was directed into an air/acetylene flame for LEI spectrometry. A repetition rate of 30 Hz was used for all LEI experiments.

Burners

Two different burners (both designed in this laboratory) were examined in this work. The first burner design (Figure 7) consisted of a Teflon base and a 2 7/8 in. diameter brass top. A flow of argon carried the vaporized sample up through a central stainless-steel capillary (o.d.=1/8 in, i.d.=1/16 in) where the sample was injected up into the flame. Premixed air and acetylene flowed up in stainless-steel capillaries (o.d.=3/32 in, i.d.=1/32 in) surrounding the central capillary and were ignited to form the flame.

Figure 6. Block diagram of the experimental setup for LEIS

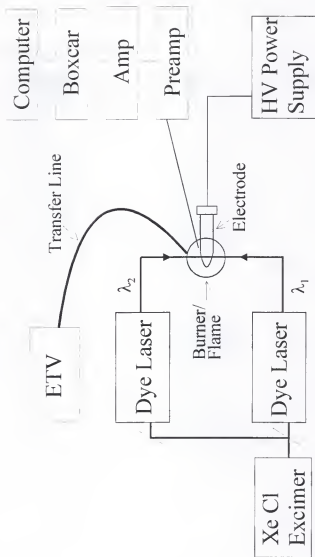
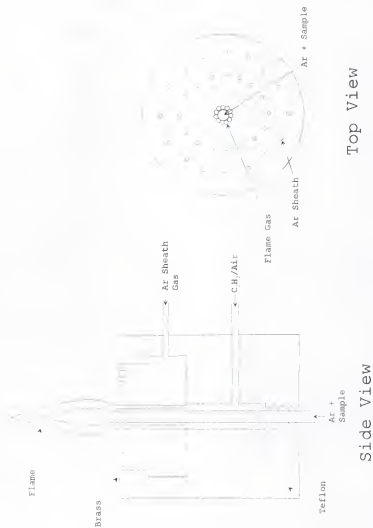


Figure 7. First burner design used for LEIS



Additional argon flowed up through 1/32 in. holes in the brass burner top to form an argon sheath around the flame.

A second burner was designed because of the large flame noise associated with the first burner design. The second burner was designed to try and minimize the flame noise by miniaturizing the burner and, hence, the flame. This second burner design (Figures 8 and 9) consisted of a bakelite body and a stainless-steel rod (1/2 in. diameter) press fit into the bakelite. A 1/8 in. hole was drilled into the stainless-steel rod and a 0.095 inch stainless-steel central capillary was inserted. A flow of argon carried the vaporized sample up the central capillary where the sample was injected up into the flame. Premixed air and acetylene flowed up in the space between the central capillary and the stainless-steel rod and was ignited to form the flame.

Graphite Furnace

A graphite furnace (System 3000, GBC Scientific Instruments, Melbourne, Victoria, Australia), modified by Finnigan (Finnigan MAT/SOLA, Bremen, Germany) for use with an ICP-MS, was used to vaporize all samples for flame LEI. Pyrolytically coated graphite tubes (Part # 4090-73, CPI, Santa Rosa, CA) were used for all graphite furnace-LEI experiments. The temperature of the graphite furnace was monitored by measuring the emission from the heated graphite

Figure 8. Diagram of new burner design with relative position of the high voltage electrode and laser beams

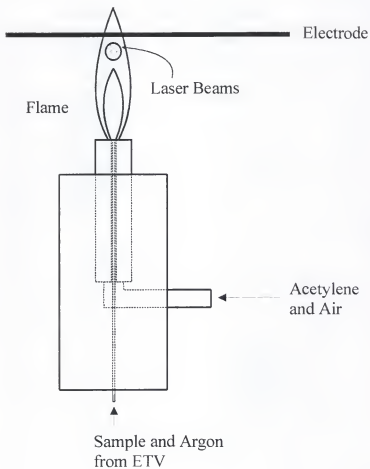
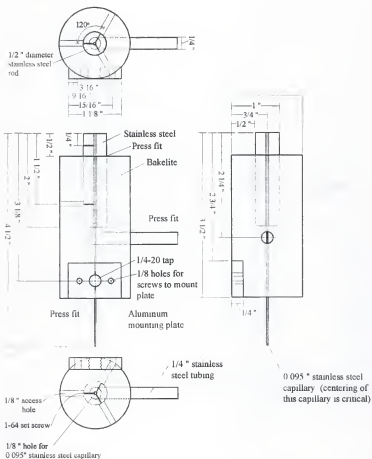


Figure 9. Detailed drawing of the new burner design



tube with a photodiode mounted just outside the right window. The vaporized sample was transferred from the graphite furnace to the burner by a flow of argon through a PTFE transfer tube (Cat. # AP-06375-02, Cole-Parmer Instrument Company, Niles, IL) approximately 1.7 m long (i.d.=5/32 in, o.d.=1/4 in), which was connected to another piece of PTFE tubing (i.d.=3/32 in, o.d.=1/8 in) by a Teflon reducing union (1/4 in to 1/8 in, Swagelock Co., Solon, OH). The 1/8 in. tubing was fitted onto the central capillary of the burner with the newer burner design.

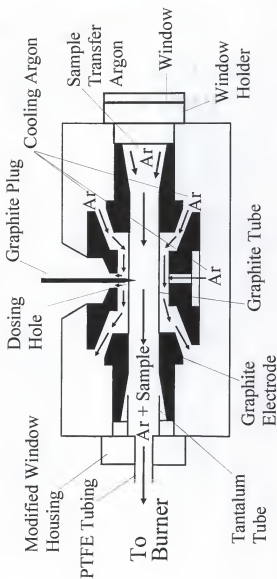
The furnace modifications made by Finnigan included separating the argon flow through the center of the graphite tube from the flow around the tube and replacing the left window of the furnace with a sample transfer interface. The argon flow through the graphite tube was adjusted with a mass flow controller. The sample transfer interface consisted of a tantalum tube placed about 5 mm from the graphite tube, a stainless-steel holder that fitted into the original window housing, and a PTFE adapter to connect the holder to the transfer tubing.

This interface was further modified in our laboratory. The tantalum tube was extended to within 2 mm of the graphite tube and the PTFE adapter was eliminated by threading the transfer tubing such that the tubing could be directly attached to the stainless-steel holder. A sharpened 1/8 in.

diameter graphite electrode (Part # L4236, Spectrographic Services, Sussex, NJ) was used to plug the injection hole of the graphite tube during heating of the graphite furnace. Figure 10 shows a cross-sectional view of the graphite furnace with the tantalum extraction probe on the left.

A water-cooled stainless-steel electrode (o.d.=3 mm) was immersed in the flame and a negative high voltage (-800 V) applied. The high voltage was optimized by adjusting the voltage until the signal-to-noise ratio was a maximum. An aluminum box was used to partially shield the system from extraneous radio frequency (rf) noise. The laser-induced charge was collected through an electrical connection to the central burner capillary and transferred to a circuit consisting of a 10 k Ω resistor to ground and a 1 nF capacitor in series. The signal then passed through a transimpedance amplifier (Model A1, THORN EMI Gencom, Fairfield, NJ), low noise amplifier (Model SR560, Stanford Research Systems, Sunnyvale, CA), and a boxcar averager (Model SR250, Stanford Research Systems, Sunnyvale, CA). The signal from the boxcar was collected on a notebook personal computer (Model Highscreen 386SX/33, Highscreen Computer, Würselen, Germany) through a computer interface (Model SR245, Stanford Research Systems, Sunnyvale, CA) using the Stanford data collection program (SR 265 v. 3.1x, Stanford Research Systems, Sunnyvale,

Figure 10. Cut-away view of the graphite furnace showing the tantalum sample extraction interface



CA). A gate width of ~800 ns was used on the boxcar.

Procedure and Conditions

For graphite furnace-LEI of magnesium, Coumarin 153 and Coumarin 120 (Lambda Physik, Acton, MA) were the laser dyes used. Both dyes were dissolved in high purity methanol (Optima grade, Fisher Scientific, Pittsburgh, PA) to the concentrations specified by the manufacturer. The output of the Coumarin 153 at 570.4 nm was frequency doubled with a BBO III crystal (Lambda Physik, Acton, MA) to provide optical excitation at 285.2 nm. The output of the Coumarin 120 provided optical excitation at 435.2 nm. Laser pulse durations were approximately 40 ns (full width at half maximum), rather than the LPX-240i nominal duration of 14 ns. Pulse energies were typically 150 mJ for the excimer, 3 mJ for the Coumarin 153, 50 μ J for λ_1 (Coumarin 153 doubled by BBO III), and 4 mJ for λ_2 (Coumarin 120). Conversion efficiencies were typically 8% for Coumarin 120, 6% for Coumarin 153, and 2% for the BBO III crystal. λ_1 [285.213 nm: $3s^2\ ^1S_0 \rightarrow 3s(^2S)3p\ ^1P_1^0$, $A_{21} = 4.95 \times 10^8\ s^{-1}$] was focused into a 5 times beam expander (Model 15600, Oriel Corporation, Stratford, CT) by a quartz cylindrical lens [focal length (f1) = 3.5 in]. λ_2 [435.191 nm: $3s(^2S)3p\ ^1P_1^0 \rightarrow 3s(^2S)6d\ ^3D_2$, $A_{32} = 2.1 \times 10^7\ s^{-1}$] was focused with a quartz lens (f1 = 41 in) into the flame.

At the flame, λ_1 is a square beam approximately 4 mm wide and λ_2 is a round beam approximately 6 mm in diameter encompassing λ_1 . Both laser beams were positioned immediately below the high voltage electrode for efficient charge collection.

The vaporization temperature for Mg was optimized by increasing the furnace temperature until no cleaning peak was observed. The graphite furnace temperature program used for magnesium is shown in Table 2. Aqueous Mg standards were prepared by diluting a stock solution (1000 $\mu\text{g/mL}$) with ultra pure 2% nitric acid (Optima grade, Fisher Scientific, Pittsburgh, PA). Sample volumes of 10 μL were used for all injections. Injections were performed using a digital pipette (Eppendorf Model 4810, Brinkman Instruments, Inc., Westbury, NY). It was observed that at concentrations of Mg below 100 ppb, the precision was worse than that observed for the higher concentrations. Therefore, the feasibility of using a matrix modifier to act as a carrier for the lower concentration samples was evaluated. The main criterion for choosing a matrix modifier was that it should not contribute a substantial Mg signal (less than our blank contamination of about 3 pg/mL). Ultra pure methanol (Optima grade, Fisher Scientific, Pittsburgh, PA) was used as a carrier for the lower concentrations of Mg. Analysis of the methanol

Table 2. Graphite furnace temperature program for magnesium

Step	Temperature (°C)	Ramp time (s)	Ramp hold (s)
1. Drying	90	10	60
2. Cool Down (add carrier)	20	10	90
3. Vaporization	2000	3	6
4. Cool Down	20	1	20
5. Cleaning	2500	3	6
6. Cool Down	20	1	10

indicated no detectable Mg was present. However, a blank LEI signal (not due to Mg) was observed with the methanol carrier. This signal was reproducible and was therefore subtracted from the sample peaks. An optimal injection volume of 6 μL of methanol was determined by optimizing the Mg LEI signal while minimizing the blank contribution. The methanol was injected after the drying step before the vaporization step.

All gas flows were optimized using the signal-to-noise for the Mg LEI signal. The gas flows were optimized by adjusting each of the flows separately and then confirming each setting after the initial optimization. Gas flow rates of 622 cm^3/min for air, 85 cm^3/min for acetylene, and 357 cm^3/min for the carrier argon were found to be optimal for Mg.

For graphite furnace-LEI of lead, Coumarin 153 and Coumarin 307 (Lambda Physik, Acton, MA) were the laser dyes used. Both dyes were dissolved in high purity methanol (Optima grade, Fisher Scientific, Pittsburgh, PA) to the concentrations specified by the manufacturer. The output of the Coumarin 153 at 566.6 nm was frequency doubled with a BBO III crystal (Lambda Physik, Acton, MA) to provide optical excitation at 283.3 nm [λ_1 , $6p^2\ ^3P_0 \rightarrow 7s\ ^3P_1^0$]. A linewidth of $0.15\ \text{cm}^{-1}$, typical pulse energy of 20 μJ , and approximate beam diameter of 1 mm were measured for the first dye laser using Coumarin 153. The Coumarin 307 was used with a different dye

laser (Model DL-14, Laser Photonics, Orlando, FL) and provided optical excitation at 509.0 nm [λ_2 , 7s $^3P_1^0 \rightarrow 8p \ ^3D_2$]. A linewidth of 0.4 cm⁻¹, typical pulse energy of 1.2 mJ, and approximate beam diameter of 5 mm were measured for the second dye laser using Coumarin 307.

The graphite furnace temperature program used for lead in blood is shown in Table 3. The vaporization temperature was optimized using the same procedure as for Mg (see above). The second ashing temperature was optimized by using the highest temperature without loss of lead during the ashing. Aqueous lead standards were prepared by diluting a stock solution (1000 µg/mL) with ultra pure 2% nitric acid (Optima grade, Fisher Scientific, Pittsburgh, PA). A 100 mg/dL sodium solution, used as a carrier, was prepared by dissolving high purity NaCl (Alfa Aesar, Ward Hill, MA) in ultra pure water (Millipore, Bedford, MA). The concentration of the NaCl was optimized by optimizing the signal-to-noise ratio for the lead LEI signal. Injection volumes of 10 µL were used for all samples, standards and the carrier. Injections were performed using a digital pipette (Eppendorf Model 4810, Brinkman Instruments, Inc., Westbury, NY).

All blood samples and standards were prepared as follows. Vials of blood were allowed to thaw completely at room temperature. The vials were then rolled carefully between

Table 3. Graphite furnace temperature program for lead in blood

Step	Temperature (°C)	Ramp time (s)	Ramp hold (s)
1. Drying	90	5	40
2. Ashing 1	260	10	10
3. Ashing 2	450	5	15
4. Vaporization	1900	3	8
5. Cleaning	2500	3	6

hands and placed in a sonicator to ensure thorough mixing. A volume of 50 μL whole blood was pipetted into a vial containing 1 mL of ultrapure water. The vials containing the diluted blood were also rolled and sonicated for thorough mixing. All blood samples and standards were refrozen immediately after use. It should be noted that the dilution of the whole blood with ultra pure water was needed only to facilitate pipetting into the graphite furnace. If an adequate pipet was available to inject whole blood into the graphite furnace, this dilution should not be necessary. Blood lead standards from the CDC and NIST were used. The standards from the CDC's Blood Lead Laboratory Reference System (BLLRS) program that were analyzed included pool ID# 694 (0.7 $\mu\text{g/dL}$), 192 (3.9 $\mu\text{g/dL}$), 1291 (10.6 $\mu\text{g/dL}$), 0191 (19.3 $\mu\text{g/dL}$), and 1092 (61.6 $\mu\text{g/dL}$). The standards from NIST included SRM 955a-1 (5.01 $\mu\text{g/dL}$), -2 (13.53 $\mu\text{g/dL}$), -3 (30.63 $\mu\text{g/dL}$), and -4 (54.43 $\mu\text{g/dL}$). One human blood sample of unknown lead concentration was also analyzed.

Flame Gas Flows, Velocity, and Temperature

All gas flows were calibrated with a mass flowmeter (Model ALK-50K, Teledyne Hastings-Raydist, Hampton, VA) at experimental conditions by inserting the mass flowmeter

between the rotameter and burner for each gas.

Average flame gas velocity was measured by observing the LEI signal at two different positions in the flame and measuring the time differential between the two ion pulses [144]. For this experiment, the burner head was grounded and an iridium wire (diameter = 0.012 in) was inserted into the flame above the laser beams (no potential applied). The Ir wire was connected to the circuit and transimpedance amplifier used for the regular LEI experiments described above. The amplified signal was observed and recorded on a digital storage oscilloscope (Model 620A, Tektronix, Beaverton, OR). Ion pulses for 10 μ L samples of 100 ppb Mg solution were observed on the oscilloscope. The Ir wire was moved a distance, d , of 1 mm in the z -direction (up and down) and the time differential, Δt , between the ion pulses was determined. The flame gas velocity was calculated by the following formula:

$$v = \frac{d}{\Delta t} \quad (42)$$

where v is the flame gas velocity (cm/s).

Flame temperature was measured using the two-line emission method [145,146] with iron. This procedure has been described in detail elsewhere [147]. All iron solutions were

introduced into the miniature flame using a laboratory constructed ultrasonic nebulizer (Figure 11). Iron emission was collected with a quartz lens ($f_l = 3.5$ in.) and focused onto the monochromator (Model EU-700, GCA/McPherson Instruments, Acton, MA) slit. The relative line intensities of Fe emission at 382.043 nm and 371.994 nm were measured. The absolute temperature, T , can be calculated from the equation:

$$T = \frac{0.6247 (E_1 - E_2)}{\log \left(\frac{g_1 A_1 v_1 I_2}{g_2 A_2 v_2 I_1} \right)} \quad (43)$$

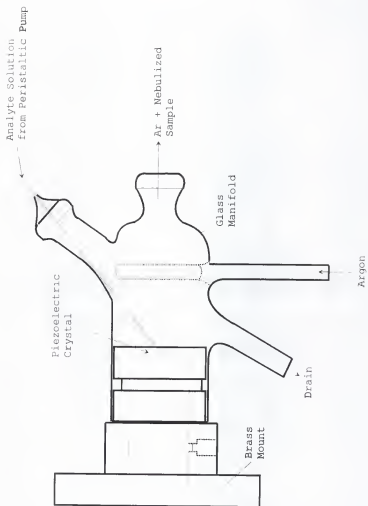
where E_1 and E_2 are the excitation energies (cm^{-1}), g_1 and g_2 are statistical weights of the states, A_1 and A_2 are transition probabilities for the lines, v_1 and v_2 are frequencies of the lines, and I_2 and I_1 are the relative intensities of the two lines.

Noise study

For all of the noise studies, five different noises were measured: the boxcar noise, the boxcar with transimpedance amplifier (A1) noise, the "DC" background, the background with rf noise, and dry run noise.

To measure the boxcar noise, the input of the boxcar was

Figure 11. Sketch of laboratory constructed ultrasonic nebulizer used



electrically shorted while data was taken. For the boxcar with A1 noise, the boxcar and A1 were connected as usual but the A1 input was capped while data was taken. The previous two noises should be the only noises associated with the electronics and should also be the same for all experiments with the different burners and flame gases.

The "DC" background noise or flame noise is the noise associated with the flame and will vary with the flame gas composition and the size of the flame. This noise was recorded with the system ready for LEI (flame lit and high voltage applied to the electrode) except that the lasers were not firing. The background with rf noise is simply the "DC" background noise with the lasers firing, so any rf noise from the lasers should be included in this noise. The dry run noise is the same as the background with rf noise except with the graphite furnace firing (no sample injected) as during a normal LEI experiment.

The noise of the first burner design was compared to the new burner design. Also, the hydrogen/air flame was compared to the acetylene/air flame for LEI of magnesium.

Fluorescence Dip and Fluorescence Profile of Flame

According to Omenetto et al.[148], when the second excitation reaches a level close to the ionization continuum

from which collisional ionization occurs very rapidly, the ionization yield can be determined by measuring what is known as the fluorescence dip. This parameter describes the decrease in resonance fluorescence from the first excited level that occurs when adding a second pumping process. This second excitation process depletes the atomic population of the first excited level such that they do not return to the ground state. The resonance fluorescence signal is always proportional to the number density of excited atoms in the first excited state [149]. As it has been shown from simple theoretical considerations [20,48,62], the ionization yield will approach unity when an optically saturating laser pulse has a duration that significantly exceeds the reciprocal of the effective ionization rate of the laser populated excited state. However, before using the fluorescence measurement to directly evaluate the ion yield, one must be sure that there is no loss due to quenching collisions into a metastable level. In the absence of collisional quenching, the ionization yield, Y_1 , can be calculated as:

$$Y_1 = \frac{I_{21}(\lambda_1 \text{ only}) - I_{21}(\lambda_2 \text{ added})}{I_{21}(\lambda_1 \text{ only})} \quad (44)$$

where I_{21} is the signal intensity for the resonance fluorescence.

For both fluorescence experiments, the monochromator was

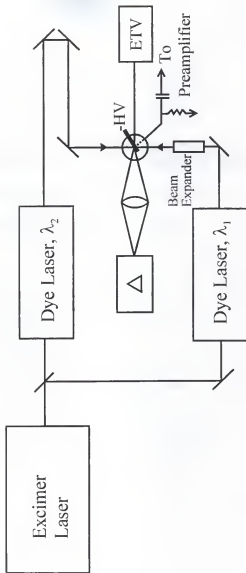
positioned at an angle of 90° from the laser beams (Figure 12). For the fluorescence dip experiments, the resonance fluorescence for Mg at 285.213 nm was collected using a quartz lens ($f_l = 3.5$ in.) and imaged onto the monochromator slit. The LEI signal was monitored simultaneously as shown in Figure 12. First, the blank (ultra pure water) signal was measured to determine the scatter (background) from the laser. Next, a solution of 10 ppb Mg was injected in volumes of 10 μL . The resonance fluorescence was first measured with only λ_1 (285.213 nm) and then remeasured with λ_2 (435.191 nm) added. The fluorescence dip was calculated from these measurements which was used to estimate the ionization yield.

A profile of the relative atom concentrations in the flame was obtained by observing the saturated resonance fluorescence (285.213 nm) at various positions in the flame. For any given spectral line of a metal vapor in a flame of constant composition and temperature, the fluorescent intensity, I_f , is given by [150]:

$$I_f = C P^* N_0 \quad (45)$$

where C is a constant term, P^* is the incident radiant power, and N_0 is the ground state concentration of the absorbing atoms. When full saturation is attained, the fluorescence signal becomes insensitive to variations in the laser power

Figure 12. Block diagram of experimental setup for monitoring of both fluorescence and LEI signals



[5]. Therefore, the concentration of Mg atoms is directly proportional to the saturated resonant fluorescent intensity.

The beam expander and cylindrical lens were removed from λ_1 (285.213 nm) for the fluorescence experiment. A planoconvex quartz lens ($f_l = 4.5$ in) was then inserted in order to focus the beam down to a very small spot in the flame. Resonance fluorescence was again collected at 90° with a quartz collection lens ($f_l = 3.5$ in) which was used to image the flame onto the monochromator slit. Saturation of the fluorescence was confirmed by insertion of neutral density filters into the excitation beam. Saturation was confirmed at several different positions within the flame. The burner was translated in the x-, y-, and z-directions and a relative spatial distribution of Mg atoms in the flame was obtained from the relative fluorescence intensities.

Transport Efficiency

In order to determine the transport efficiency from the furnace to the flame, a trapping technique modelled after that described by Schmertmann et al. [151] was used. It should be noted that the efficiency measured here includes the vaporization efficiency of the furnace. It was assumed that the vaporization efficiency of the furnace was 1.000 (± 0.001)

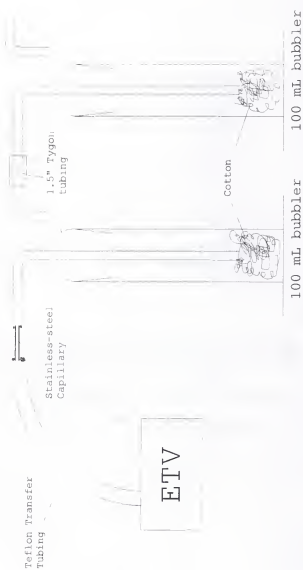
since no observable cleaning peak was obtained with the optimized vaporization temperature.

A sketch of the experimental setup is shown in Figure 13. Cotton was used to trap the particulates transported from the furnace by the flow of argon. Various types of cotton were digested in 50% high-purity nitric acid (Optima grade, Fisher Scientific, Acton, MA) and analyzed by flame-atomic absorption to determine the cotton with the lowest Mg impurity. PADCO cotton (Non-surgical bleached cotton, ACCO, Valley Park, MO), purchased from Fisher Scientific was found to have the least Mg impurity and was selected for use.

The trapping apparatus consisted of two glass bubblers connected in tandem to the end of the transfer tubing leading to the burner. The connection between the tubing and the first bubbler included a one inch length of stainless-steel capillary to make it as similar as possible to the connection between the tubing and the mini-burner. The connection between the two bubblers was a two-inch length of Tygon tubing (i.d.= 0.375 in, o.d.= 0.625 in). A 1.60 g sample of the cotton was placed into the bottom of each bubbler to trap the particulates produced by the furnace.

Since the resulting trapping solution was to be analyzed by atomic absorption, the final concentration had to be in the range of 1-1000 ppb. This was achieved by the injection of

Figure 13. Sketch of experimental setup for transport efficiency measurement



100 samples of 100 ppm Mg solution (10 μ L each). The cotton was then digested in 60 mL of 50% high-purity HNO_3 in a 70°C water bath for 30 minutes. The resulting solution was then hot filtered into a 100 mL volumetric flask and diluted to the mark with ultra pure water.

To confirm the validity of the trapping technique, the LEI system was used to analyze Mg standards from 1 ppb to 100 ppm which indicated that the signal remained linear over this range. The burner was connected to the end of the trapping system for LEI analysis of any Mg that made it through the trapping system. A >99.9% reduction in the LEI signal for a 100 ppm Mg sample confirms that the Mg is not escaping from the trap.

In an effort to account for the analyte losses incurred during transport, an analysis of the residue in the transfer tubing was performed. The transfer tubing was rinsed with 50% high-purity HNO_3 and the subsequent solution analyzed by atomic absorption and LEI. To estimate the loss of Mg due to diffusion through the graphite tube, the shroud gas flowing around the outside of the graphite tube and out through the dosing hole opening was diverted into the flame for LEI analysis. The argon flow was adjusted to match the flow through the inside of the graphite tube. A small piece of graphite was used to plug the dosing hole. It should be noted

that this diffusion loss experiment may tend to overestimate the losses due to diffusion through the graphite tube. This is because the graphite plug was not held in place within the dosing hole. Therefore, significant amounts of Mg may have leaked out through the dosing hole. During the LEI experiments, the graphite plug is securely held in place by an aluminum holder.

Transimpedance Amplifier Calibration

The theoretical detection limit of the transimpedance preamplifier was calculated by determining the equivalent noise charge (ENC) of the preamplifier [152]. A pulse generator (Model PG501, Tektronix, Beaverton, OR) was connected to the input circuit consisting of a capacitor, C_a , (1 pF) which was connected in series to the Thorne A1 preamplifier. Some parasitic or stray capacitance, C_p , in parallel was also present in the circuit. The value of C_p is typically around 15 to 30 pF. An input voltage, U_{in} , of 55.4 mV (50 ns pulse width) was delivered by the pulse generator. If $C_p \gg C_a$, then $Q_c = U_{in} \cdot C_a$ where Q_c is the charge. The ENC can be calculated by the equation:

$$ENC = \frac{Q_c S_N}{S_p} = \frac{U_{in} C_a S_N}{S_p} \quad (46)$$

where S_N is the RMS noise of the preamplifier and S_p is the output of the preamplifier. To determine S_N , the preamplifier input was disconnected and the RMS noise of the preamplifier measured using an oscilloscope.

The charge response of the detection system was measured using the following scheme. The pulse generator described above was connected to a calibration circuit consisting of a $50\ \Omega$ resistor in parallel and a capacitance, C_c , in series. A parasitic or stray capacitance, C_p , was again present in parallel within this circuit. The calibration circuit was then connected to the original input circuit and the A1 preamplifier. A voltage pulse, U_{in} , was applied and the output of the preamplifier, S_p , was measured for each value of C_c . If $C_p \gg C_c$, then $Q_c = U_{in} \cdot C_c$ where Q_c is the charge applied. Values of 1 pF and 2 pF were used for C_c . A 55.4 mV pulse was used for U_{in} (50 ns pulse duration). The average signal output, S_p , from the preamplifier corresponding to a 1 pF charge was recorded. The amount of charge, Q_c , was calculated and divided by S_p to give the charge response of the detection system.

Atomization Efficiency Measurement

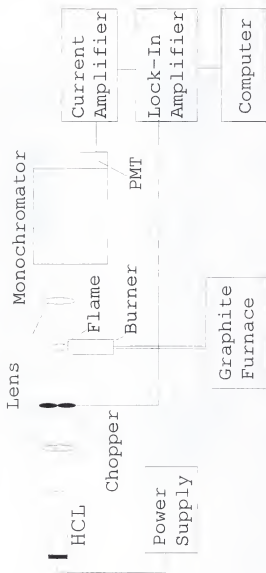
The determination of atomization efficiencies by an absorption measurement in the flame has been described by

others [5]. A block diagram of the experimental setup used for the determination of the atomization efficiency for Mg is shown in Figure 14. The emission from a Mg hollow cathode lamp (Varian, San Fernando, CA) with power supply (Model EU-703-62, Heath, Benton Harbor, MI) was modulated with a mechanical chopper (Model SR540, Stanford Research Systems, Sunnyvale, CA) and then imaged onto the flame with a planoconvex quartz lens ($f_l = 4.5$ in). The transmitted light was then imaged onto the monochromator (described earlier) slit with a biconvex quartz lens ($f_l = 3.5$ in). The photomultiplier tube (Model R928, Hamamatsu Photonics, Bridgewater, NJ) output was sent to a current amplifier (Model 427, Keithley Instruments, Cleveland, OH). The amplified signal was then sent to a lock-in amplifier (Model 5207, EG&G Princeton Applied Research, Princeton, NJ) and collected on a personal computer (described earlier). The burner and graphite furnace were the ones used for graphite furnace-LEI experiments. The absorption at 285.213 nm for Mg was measured.

The absorbance at the line center, $A(v_0)$, is related to the total number density, n_T , of Mg atoms by [5]:

$$A(v_0) = 1.15 \times 10^{-2} \frac{g_0}{Z(T)} \frac{f n_T l}{\Delta v_{eff}} \quad (47)$$

Figure 14. Block diagram of the experimental setup for the determination of the atomization efficiency for Mg by atomic absorption



where g_0 is the statistical weight of the ground state, $Z(T)$ is the electronic partition function, f is the absolute oscillator strength, l is the absorption path length, and $\Delta\nu_{eff}$ is the effective line width of absorption.

CHAPTER 6 RESULTS AND DISCUSSION

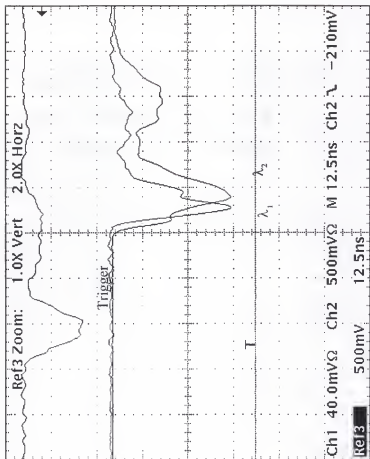
LEI of Magnesium

After the system was assembled as described in Chapter 5 with the first burner design, the laser beams were aligned to be coincident in space and time. The oscilloscope trace shown in Figure 15 shows the coincidence of the laser beams in time and was taken with a fast photodiode (Model ET2000, Electro-Optics Technology, <200 ps risetime, Fremont, CA) and the oscilloscope described earlier. From the trace, there appeared to be good temporal overlap of the two laser beams even though the maximum intensity for λ_1 appears slightly before the maximum for λ_2 .

Magnesium as Analyte

Once the lasers were aligned, the ETV-FL-LEI system was characterized with magnesium. Magnesium was chosen as the analyte because Mg had been analyzed successfully by graphite furnace LEI previously in our laboratory [4] and was being analyzed by graphite furnace (electrothermal vaporization

Figure 15. Oscilloscope trace of the laser beam timing



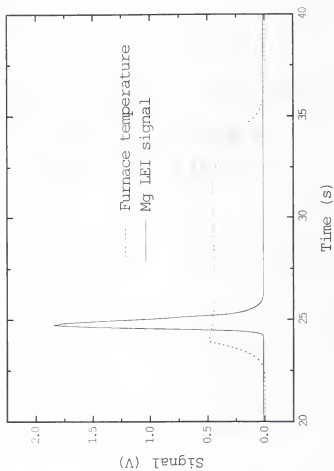
ETV-ICP-MS also in our laboratory [153] employing the same graphite furnace design. However, it was found throughout the course of our research with LEI that there are several difficulties associated with Mg. Due to the relative abundance of Mg in nature, sample contamination was significant. Regular laboratory glassware could not be used for sample preparation and storage. Instead, plastic or Teflon volumetric flasks, pipettes, and storage bottles that were carefully soaked and cleaned in high-purity nitric acid and ultra pure water were used. These precautions appeared to reduce sample contamination below the blank level.

There was also difficulty in finding a matrix modifier/carrier for use with low Mg concentrations. The inorganic matrix modifiers examined all contained significant amounts of Mg impurity. Most of the organic matrix modifiers examined produced laser-induced ionization signals most likely from molecular species. Finally, the limit of detection for Mg would ultimately be limited by the blank signal since the stock nitric acid solution used to prepare standards and samples contains ~0.02 ppb Mg.

Mg LEI Signal

A typical LEI signal for Mg is shown in Figure 16. The second trace is the signal from the photodiode monitoring the furnace temperature. There is a ~0.4 s time differential

Figure 16. Typical LEI signal for magnesium with older burner



between when the furnace reaches the vaporization temperature and the appearance of the LEI signal. This is the sample vapor transit time from the furnace to the flame. The Mg LEI signal lasts ~1.5 s and ends well before the end of the furnace vaporization cycle.

An important issue for applying LEI to standardless or absolute analysis is the conversion of the collected signal, in volts, to the induced charge, in coulombs, created in the flame. For a successful conversion, the charge response of the detection system must first be calibrated. The procedure used to measure the charge response was outlined in the previous chapter. The signal, S_p , corresponding to an input potential of 55.4 mV and a capacitance, C_e , of 1 pF was found to be 10.5 mV. The applied charge, Q_e , of 5.5×10^{-14} C (3.44×10^5 electrons) was divided by the signal, S_p , to obtain the charge response of 5.2×10^{-15} C/mV (3.3×10^4 electrons/mV).

The output of the boxcar (in mV) was divided by the gain of the amplifier and then multiplied by the charge response of the detection scheme (input circuit and A1 transimpedance amplifier) which gives the charge (in C) produced by each laser pulse. These were summed over the duration of the Mg LEI peak to give the total charge collected that was produced by the given Mg sample.

System Parameter Optimizations for Old Burner Design

Next, the system parameters were optimized for Mg. The results of the transfer argon flow rate optimization are shown in Figure 17. At low Ar flow rates (≤ 0.6 L/min), the precision of the signal was poor. This was due to broadening of the sample peaks and the difficulty in determining where peaks began and ended. At high Ar flow rates (≥ 1.5 L/min), the sampling efficiency of the laser beams was decreased because the analyte passed by too quickly. The optimal Ar flow rate of 0.9 L/min was chosen because the best combination of signal intensity and precision were obtained at this flow rate.

The results of the optimization of the distance between the burner and electrode are shown in Figure 18. When the burner and electrode were close together (2.7 cm), the signal was lower because the argon and sample vapor did not have enough time to thoroughly mix with the flame gases. As a result, the sample was not well atomized by the flame and hence the lower signal. When the electrode and burner were far apart (4.7 cm), the Mg atoms began to dissipate. Lower field strength may also have contributed to the rapid reduction in signal. An optimal burner-to-electrode distance of 3.2 cm was chosen because the optimal combination of Mg-LEI signal intensity and precision were obtained at this distance.

The results of the optimization of the voltage applied to the LEI electrode are shown in Figure 19. The signal

Figure 17. Argon flow rate optimization for Mg with older burner

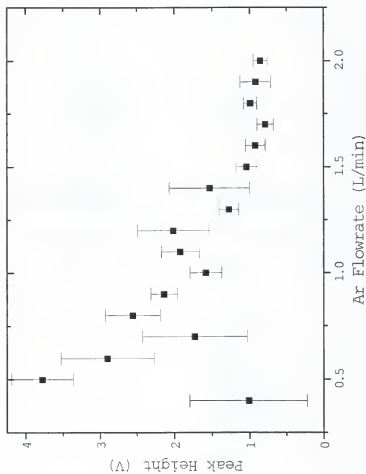


Figure 18. Burner-to-electrode distance optimization for Mg with older burner

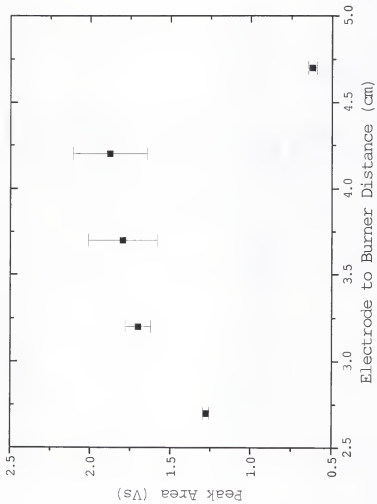
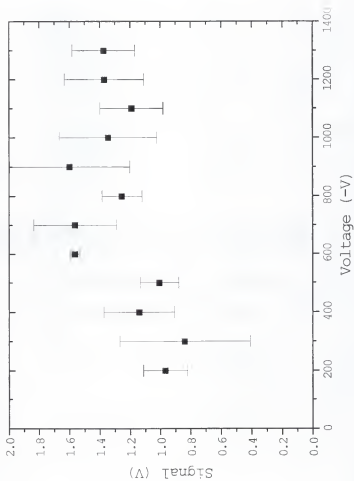


Figure 19. Applied voltage optimization for Mg with older burner



increases as the applied voltage increases until a plateau is reached around -600 V. The voltage applied to the electrode was chosen to be -600 V. The best combination of signal intensity and precision was obtained at this voltage.

Flame Profile With Old Burner

A horizontal profile of the flame (Figure 20) was obtained by translating the burner horizontally along the axis perpendicular to the laser beams. From the profile, it appears that the flame is approximately 8 mm wide. Since the laser beam for λ_1 is ~1 mm wide, a significant portion of the signal was being missed.

Analytical Curve With Old Burner

An analytical curve for Mg with the first burner design was obtained and is shown in Figure 21. A slope of 0.856 (± 0.009) C/mol was obtained although the linearity was not very good as seen in the Log-Log plot of Figure 22 (slope = 0.85). A 3σ detection limit of only 12 ppb Mg was calculated. The poor detection limit was partially due to the large flame background noise with this flame. Therefore, a hydrogen/air flame was examined as a possible alternative to the acetylene/air flame that was being used.

The hydrogen/air flame should have a lower temperature and thermal ionization associated with it. This should

Figure 20. Horizontal profile of the flame with the older burner

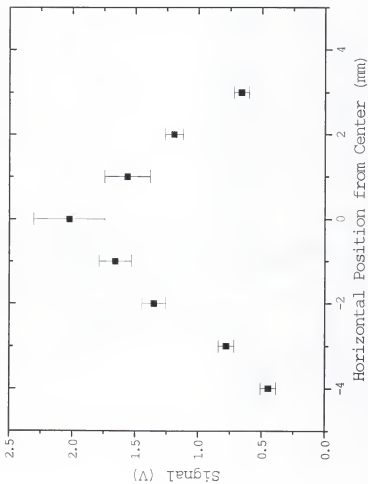


Figure 21. Analytical curve for Mg with the older burner

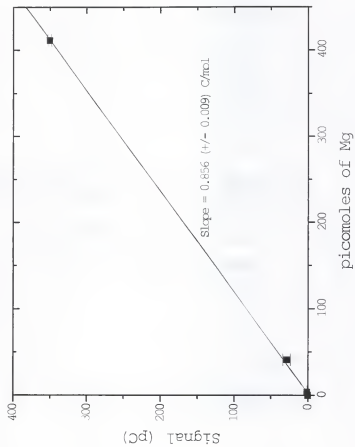
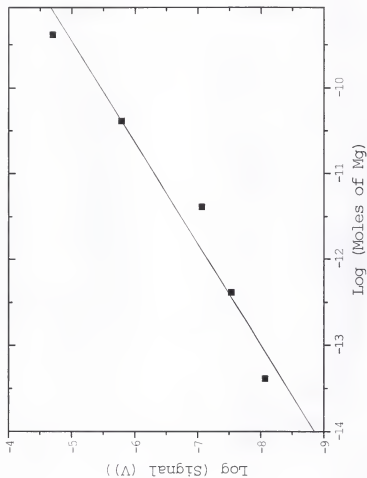


Figure 22. Log-Log plot of the analytical curve of Figure 21



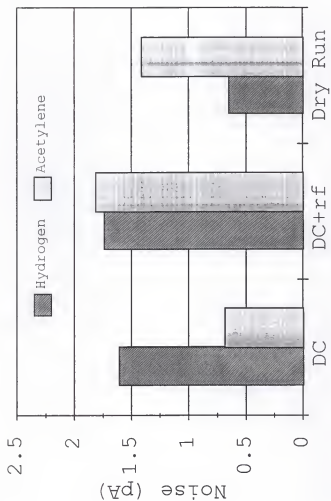
translate to a lower flame background noise. The noises of the hydrogen/air flame and the acetylene/air flame were measured and the results are shown graphically in Figure 23. From the results, it appears that the noises for the two flames are within about a factor of two of each other. The noise during the dry furnace run appears to be lower than without the furnace firing, however, within experimental error they are the same. The hydrogen/airflame was not used for Mg analysis since there was no significant lowering of the flame background noise and a 10-fold loss in sensitivity was also observed due to the lower temperature (and collisional environment) of the hydrogen/air flame.

New Burner Design

Therefore, to alleviate the large flame background noise, a new burner design was proposed and subsequently built by the departmental machine shop. This new burner was shown in Figures 8 and 9 and described in the previous chapter. An essential feature of the new burner is the much smaller dimensions of the burner and, hence, the flame. By reducing the size of the flame, it was hoped that the flame background noise would be reduced to a manageable level.

The noises of the new burner were measured as described in the previous chapter. The noises for the new burner design with an acetylene/air flame were then compared to the old

Figure 23. Noises (rms) for the hydrogen/air and acetylene/air flames with the older burner design



burner design also with an acetylene/air flame. Figure 24 shows the Log of the noises (plus 15) for the new and old burner designs. From the graph, it is evident that the noises for the new burner design are about two orders of magnitude lower than the old burner design. Therefore, a lowering of the detection limit by two orders of magnitude would be expected if the sensitivity remains the same.

System Parameter Optimizations With New Burner

The system parameters were optimized for the new burner design. The results of the argon flow rate optimization are shown in Figure 25. Once again, at the higher argon flows, the sample passes through the flame too quickly to be probed efficiently by the laser beams. At lower flow rates, the sample peaks are broad and hard to define which results in poor precision. An optimal argon flow rate of 0.3 L/min was chosen since the best combination of LEI signal intensity and precision were obtained at this flow.

The results of the flame gas optimizations are shown in Figure 26 and Figure 27. The LEI signal for Mg appeared to be fairly constant for acetylene flow rates between 80 and 100 mL/min. An optimal flow of 85 mL/min for acetylene was chosen as the best precision was obtained at this flow rate. The Mg LEI signal appeared to be constant for air flow rates between 0.55 and 0.65 L/min. An optimal flow rate of 0.62 L/min was

Figure 24. Comparison of the noises (rms) for the new and old burner designs

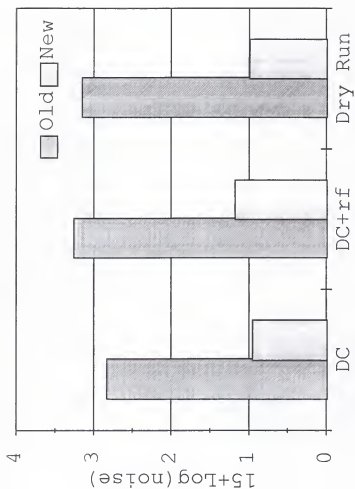


Figure 25. Argon flow rate optimization with new burner

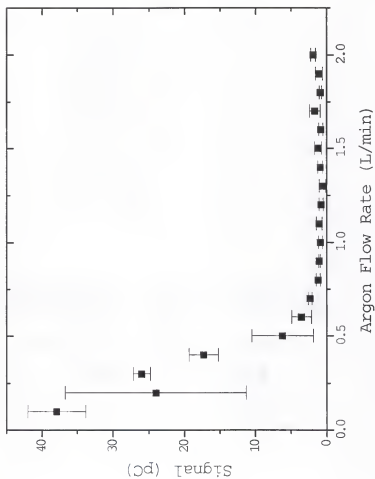


Figure 26. Acetylene flow rate optimization with new burner

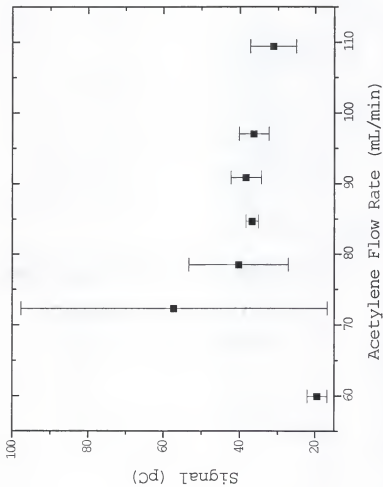
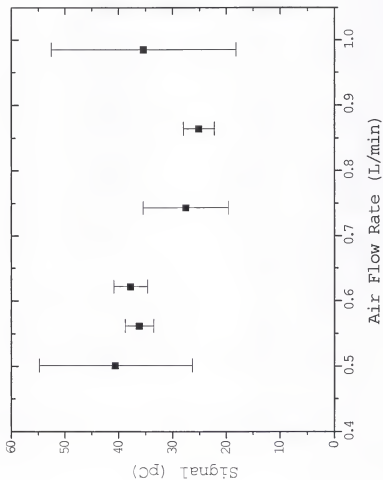


Figure 27. Air flow rate optimization for new burner



chosen because good precision and signal intensity were obtained at this flow.

The distance between the burner and the electrode was optimized as before and the results are shown in Figure 28. A burner-to-electrode distance of 14 mm was chosen since the signal reached a maximum at this distance. The voltage applied to the electrode was also optimized with the results shown in Figure 29. At about -300 V, the LEI signal reaches a plateau. A voltage of -400 V was chosen as optimal since good precision was obtained at this voltage.

Flame Profile With New Burner

A horizontal profile of the flame was measured as described previously and is shown in Figure 30. A Gaussian profile was fit to the data. If the laser beam for λ_1 is 4mm wide, then the estimated spatial probing efficiency from the data is 0.81 (± 0.05).

A spatial profile of the relative fluorescence intensities for Mg in the flame is shown in Figure 31. The fluorescence intensities can be related to the relative Mg atom concentrations in the flame. As a result, this profile gives an indication of where the Mg atoms reside in the flame. It appears that the laser beams should be centered about 10 mm above the burner head. This is expected since it should take a certain distance for the cold argon and sample to thoroughly

Figure 28. Burner-to-electrode distance optimization for new burner

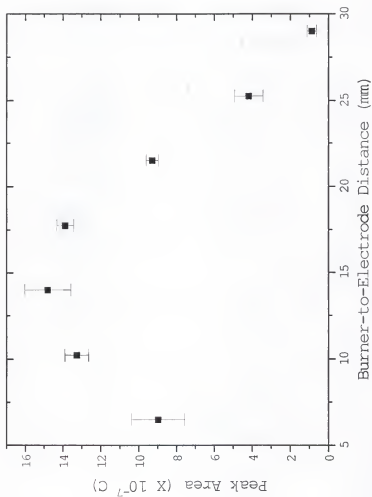


Figure 29. Electrode voltage optimization with new burner

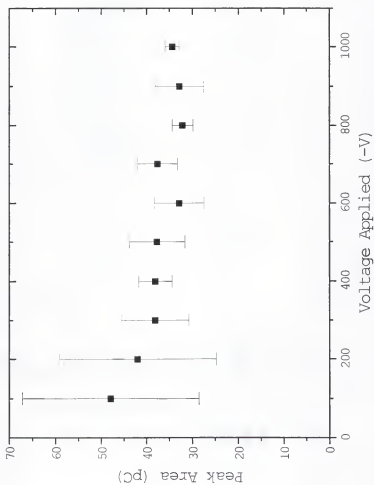


Figure 30. Horizontal profile of Mg atoms in flame with new burner

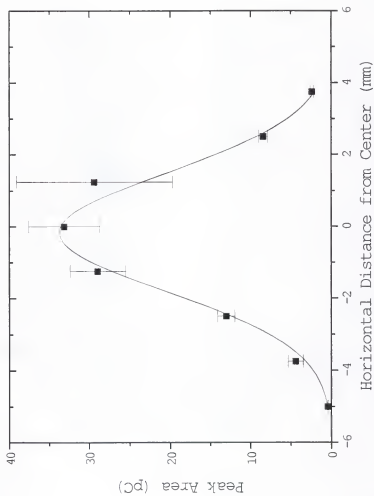
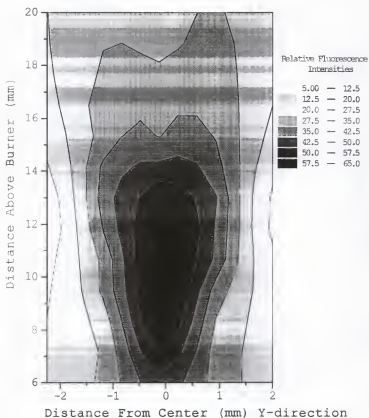


Figure 31. Fluorescence profile of Mg atoms in the flame with the new burner



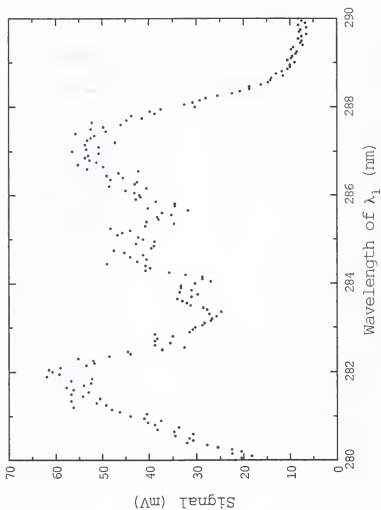
mix with the flame gases. The data shown in Figure 31 also confirm that over 80% of the Mg atoms reside within a 4 mm width. Over 99% of the Mg atoms reside within approximately a 6 mm flame diameter.

Matrix Modifier/Carrier

Once all of the optimizations were performed, solutions of different concentrations of magnesium were introduced to check the linearity of the system response. It was observed that at lower concentrations of Mg (<100 ppb), the precision was worse than that observed for the higher concentrations. Therefore, the feasibility of using a matrix modifier to act as a carrier for the lower concentration samples was evaluated.

The main criterion for choosing a matrix modifier was to find one which contributed a negligible Mg LEI signal (less than our blank signal from the HNO₃ of about 3 pg/mL). Ultra pure methanol (Optima grade, Fisher Scientific, Acton, MA) and xylene (Low trace metals grade, Mallinckrodt Chemicals, Paris, KY) were chosen as possible modifiers. Analysis of the xylene indicated a large blank LEI signal from the xylene alone. The LEI signal from xylene was then measured while scanning the dye laser for λ_1 . The results shown in Figure 32 suggest that the LEI signal is a result of molecular interferences from the

Figure 32. LEI signal for xylene while scanning dye laser for λ_1



vaporized xylene. Therefore, xylene was not used for the analysis of Mg by LEIS.

Subsequent analysis of the methanol indicated that no detectable Mg was present, but a blank LEI signal (not due to Mg) was observed with the methanol carrier. However, this signal was reproducible and was therefore subtracted from the sample signals. The effect of methanol on the Mg LEI signal is shown in Figure 33. From the plot, it appears that methanol does enhance the ionization signal for Mg, presumably by enhancing the transport of the sample vapor from the furnace to the flame. The optimal amount of methanol injected was found to be 6 μL as the best precision and enhancement of the Mg signal was observed with this volume.

Analytical Curve With New Burner

The analytical curve with methanol carrier (Figure 34) was found to be linear for 2.5 to 100 ppb of Mg in 2% HNO_3 . A slope of 2.5 (± 0.2) C/mol was obtained and the experimental limit of detection (LOD, $S/N=3$) was estimated to be 2 ng/mL (20 pg absolute). This LOD was limited by the blank signal from the 2% HNO_3 and methanol carrier.

The limiting non-blank noise level was found to be 9.8 fC rms. This limiting noise level was primarily due to rf noise from extraneous sources. Using this limiting instrumental noise, the LOD for Mg was calculated to be 29 pg/mL (290 fg

Figure 33. Effect of methanol on LEI signal for Mg

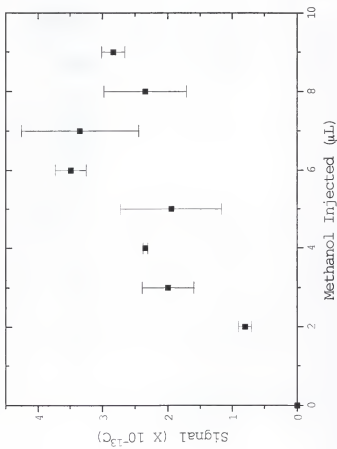
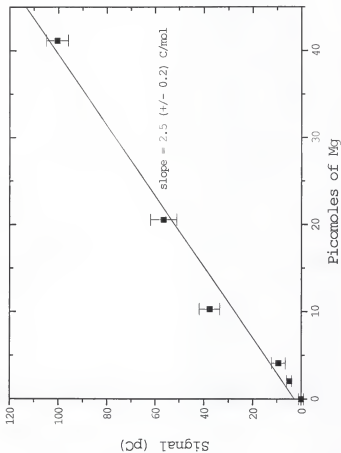


Figure 34. Analytical curve for Mg with new burner and methanol



absolute).

The extraneous rf noise may be reduced by the design and construction of a better metal shielding box. If the rf noise can be reduced to a level below that of the A1 preamplifier noise, then the theoretical LOD for Mg was calculated to be 590 fg/mL (5.9 fg absolute). This compares favorably with LODs recently determined for Mg with ETV-ICP-AES (0.1pg) [154], ETV-ICP-MS and FANES (20 pg) [155], and ETV-AAS (0.4 pg) [156].

Flame Temperature and Flame Gas Velocity With the New Burner

The flame temperature was measured using the two-line method as indicated in the previous chapter. The values for the parameters used to calculate the temperature are given in Table 4 [157]. The ratio of the intensity of the two lines, I_2/I_1 , was experimentally found to be 14.1. The value for the flame temperature was calculated to be approximately 1973°C. This is cooler than a normal air/acetylene flame (temperature 2267°C). However, this result was expected since our flame is much smaller than a typical air/acetylene flame. A stream of cold argon carrying the sample was injected up the center of the flame which may have also lowered the flame temperature.

The flame gas velocity was measured as discussed in the previous chapter. The time differential, Δt , was measured as 240 μ s for a distance, d , of 1 mm. The flame gas velocity was

Table 4. Values used for flame temperature calculation

Parameter	Value
k	$6.95197 \times 10^{-1} \text{ cm}^{-1}\text{K}^{-1}$
ν_1	$7.847 \times 10^{14} \text{ Hz}$
E_1	$33,096 \text{ cm}^{-1}$
g_1	9
A_1	$6.68 \times 10^7 \text{ s}^{-1}$
ν_2	$8.059 \times 10^{14} \text{ Hz}$
E_2	$26,875 \text{ cm}^{-1}$
g_2	11
A_2	$1.62 \times 10^7 \text{ s}^{-1}$
I_2/I_1	14.1 (measured)

then calculated to be 4.2 (± 0.1) m/s.

Absolute Analysis

Once again, in order to consider graphite furnace-flame-LEI for absolute or standardless analysis, all of the efficiencies described in Chapter 3 must be measured. Here the values for these efficiencies are reported.

Vaporization Efficiency

After the vaporization temperature was optimized, the vaporization efficiency was checked by attempting to observe the LEI signal associated with the cleaning step of the furnace temperature program. However, no signal was observed from the cleaning step even after increasing the preamplifier gain ten times. Therefore, the vaporization efficiency was assumed to be 1.000 (± 0.001).

Transport Efficiency

As indicated in the previous chapter, three different cotton samples were analyzed by Wendy Clevenger using flame-AA to determine their Mg content for potential use in the transport efficiency determination. All three cotton samples were obtained from Fisher Scientific (Acton, MA). The results of the analysis are summarized in Table 5. As indicated

Table 5. Mg concentration in different cotton samples

Sample	Concentration (ppb)
ACCO	12.5
PADCO	2.47
First Aid	21.8

before, the PADCO cotton (non-surgical bleached cotton, ACCO, Valley Park, MO) had the lowest Mg content and was chosen for use in the transport efficiency determination.

The results of the transport study indicated that the transport efficiency was 0.17 (± 0.05). It was determined that about 8% of the analyte was being lost due to adhesion to the tubing walls and about 24% due to diffusion through the graphite walls of the furnace. However, the diffusion losses may not be accurate because the dosing hole was not plugged well as indicated in the previous chapter. The rest of the analyte loss during transport was not accounted for. It is suspected that the unaccounted analyte is escaping through the 2 mm gap between the graphite tube and the tantalum tube inside the ETV.

Probing Efficiency

Once again, the probing efficiency of the laser beams, ϵ_p , is the product of the spatial probing efficiency, ϵ_s , and the temporal efficiency, ϵ_t . The spatial probing efficiency was estimated, from the fluorescence profile of the flame at a distance of 10 mm above the burner head, to be 0.81 (± 0.05). This could be improved by expanding the laser beam for λ_1 . However, expanding the beam may result in a loss of saturation for the first step from the decreased power density of the

beam. The temporal probing efficiency can be calculated from the diameter of the laser beam, the frequency of the pulsed laser, and the velocity of the flame gases. The diameter of the laser beam was 4 mm, the laser frequency used was 30 Hz, and the velocity of the flame gases was measured to be 420 cm/s. The temporal efficiency was calculated to be 0.029 (± 0.007).

To increase the temporal probing efficiency of the lasers, an increase in the repetition rate of the lasers was proposed. Figure 35 shows the intensity of the LEI signal with increasing repetition rate. It was expected that the signal would increase with increasing repetition rate until a plateau was reached when the temporal probing efficiency reached unity. However, the results showed an increase in the LEI signal until 200 Hz, where the signal dropped very rapidly. To understand why this happened, the dye laser conversion efficiencies were monitored with increasing repetition rate as shown in Figure 36 (λ_1) and Figure 37 (λ_2). From Figure 36, it can be seen that the conversion efficiency for λ_1 remained relatively stable with only a small reduction in efficiency by 250 Hz. However, from Figure 37, it can be seen that the conversion efficiency for λ_2 drops off very quickly above 100 Hz. Unfortunately, as a result, repetition rates of only up to 100 Hz can be used for Mg LEI measurements

Figure 35. Mg LEI signal with increasing laser repetition rate

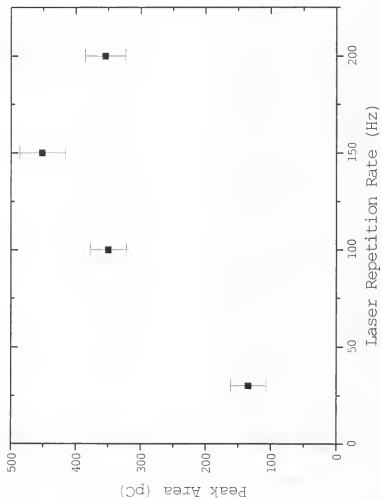


Figure 36. Dye laser conversion efficiency with increasing laser repetition rate for λ_1

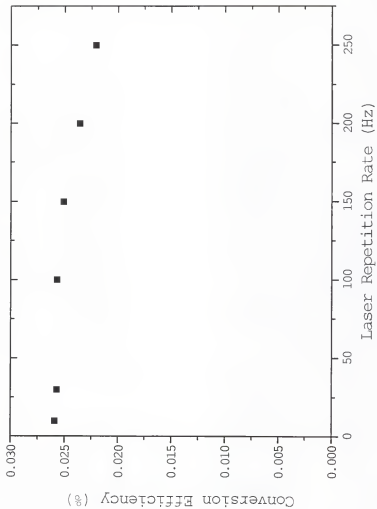
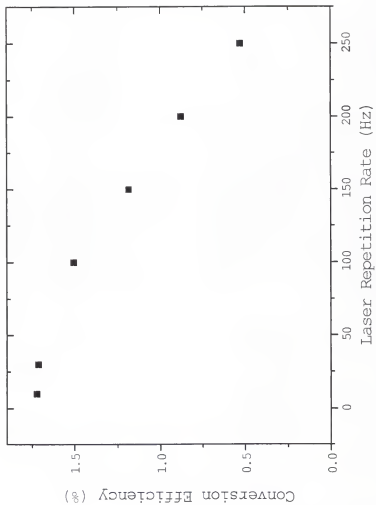


Figure 37. Dye laser conversion efficiency with increasing laser repetition rate for λ_2



with the present laser system. From these an overall laser probing efficiency for the laser beams, ϵ_p , was determined to be 0.023 (± 0.006).

Detection Efficiency

The detection efficiency, ϵ_d , is the product of the ionization yield, Y_i , and the efficiency of charge collection, ϵ_c . From the fluorescence dip experiment, when the second step was added, the result was a >99.9% dip in the fluorescence signal. This indicated a high degree of ionization within the flame, as the only other source of fluorescence dip, collisional redistribution to other excited levels, contributes <2-3%. To confirm the absence of a fluorescence signal, the gain on the boxcar was increased by a factor of ten and the measurements repeated. To confirm the absence of collisional quenching as a source of decreased fluorescence, measurements were made at several incident laser powers, confirming that near saturation was always achieved. From these results, the ionization efficiency of Mg in the flame was reported to be 0.98 (± 0.03).

The actual potential in the flame at the level of the laser beams was determined by measuring the potential using an iridium wire inserted directly into the flame. The actual potential in the flame at the height of the laser beams, ΔV ,

was found to be -540 V. The applied potential, V , was -800 V. Therefore, the efficiency of charge collection, ϵ_D , was calculated to be 0.69 (± 0.03). From these the overall detection efficiency, ϵ_d , was calculated to be 0.68 (± 0.03).

Atomization Efficiency

The atomization efficiency for Mg was measured as described in the previous chapter. The values for the parameters in Equation 45 were first determined. The statistical weight of the ground state, g_0 , is equal to 1. The electronic partition function, $Z(T)$, was calculated from the equation [158]:

$$Z(T) = 0.99101 + 0.013474(T/10^3) - 6.4659 \times 10^{-3}(T/10^3)^2 + 9.7446 \times 10^{-4}(T/10^3)^3 \quad (46)$$

where T is the temperature in K which was measured as ~ 2300 K. The value for $Z(T)$ was then calculated to be 0.99963. The absolute oscillator strength, f , was estimated to be 1.81 [159]. The absorption path length, l , was estimated to be 0.6 cm from the fluorescence profile of the flame. The effective line width of absorption, $\Delta\nu_{\text{eff}}$, was calculated by the equation [5]:

$$\nu_{\text{eff}} = \int_{\text{line}} \frac{S_\nu(\nu)}{S_\nu(\nu_0)} d\nu = \frac{1}{S_\nu(\nu_0)} \quad (47)$$

where $S_v(\nu)$ is the spectral distribution and $S_v(\nu_0)$ is the value of $S_v(\nu)$ at the line center. The spectral distribution (assuming a Voigt profile) at the line center is given by [160]:

$$S_v(\nu_0) = \left(\frac{2(\ln 2)^{1/2}}{\Delta\nu_D(\pi)^{1/2}} \right) \delta(a, 0) \quad (48)$$

where $\Delta\nu_D$ is the doppler broadening half-width and $\delta(a, 0)$ is the Voigt integral (approximation). The doppler broadening half-width is given by [161]:

$$\Delta\nu_D = 2 \left[\frac{2(\ln 2)kT}{M/(1000N_A)} \right]^{1/2} \frac{\nu_0}{c} \quad (49)$$

where k is the Boltzmann constant (JK^{-1}), T is the temperature (K), M is the atomic mass (g/mol), N_A is Avagadro's number (mol^{-1}), ν_0 is the line center frequency (Hz), and c is the speed of light (m/s). The Voigt integral may be approximated by [161]:

$$\begin{aligned} \delta(a, 0) &= (1 + 1.2a)^{-1} & \text{for } 0 < a < 2 \\ \delta(a, 0) &= (0.56/a) & \text{for } a > 2 \end{aligned} \quad (50)$$

where a is the damping constant for Mg which is ~ 0.60 for a temperature of 2333 K [161].

From the above equations, it was calculated that the total number density, n_r , is related to the absorbance at line

center, $A(v_0)$ by:

$$n_T = 1.08095 \times 10^{12} A(v_0) \quad (51)$$

The total number of atoms passing through the flame, N , is related to n_T by:

$$N = F \cdot t / n_T \quad (52)$$

where F is the total gas flow (cm^3/s). The total number of atoms passing through the flame was calculated to be 7.77×10^{11} atoms of Mg by estimating the total gas flow as the flow of the argon which was $5.95 \text{ cm}^3/\text{s}$. The total number of Mg atoms (as free atoms and molecules) reaching the flame was calculated to be 2.1×10^{13} using the transport efficiency calculated earlier. Therefore, the atomization efficiency, ϵ_a , was estimated experimentally as $0.04 (\pm 0.02)$.

An overall system efficiency was calculated as the product of each of the individual efficiencies and found to be $1.0 \times 10^{-5} (\pm 0.7 \times 10^{-5})$. If we multiply the overall efficiency by the Faraday constant ($96,485 \text{ C/mol}$), we should obtain the sensitivity of the method (slope of the calibration curve). From the calculation, a sensitivity of $9 (\pm 7) \text{ C/mol}$ was obtained. The slope of the calibration curve from the experimental results for Mg was $2.5 (\pm 0.2) \text{ C/mol}$ which is within experimental error of the calculated value. However, the error in the calculated sensitivity was large. This was

due to the large uncertainties in the values used to calculate the atomization efficiency, ϵ_a , for Mg.

Although all of the system efficiencies were determined experimentally, they do not appear to be useful for absolute analysis. The transport, probing, detection, and atomization efficiencies were all less than unity. Ideally, these should all be equal to unity for absolute analysis. Since the efficiencies are not unity, this could indicate that the efficiencies vary from sample to sample and run to run.

Also, it appears that the matrix has a pronounced effect on the transport efficiency as was evident from the need for the addition of a carrier at low Mg concentrations. Since a method must be free from matrix interferences to be considered absolute, even if the system efficiencies were improved to unity, the method would still not be considered absolute because of this matrix dependence of the signal.

LEI of Lead

Excitation Scheme for Lead

Four different two-step excitation schemes were examined for the analysis of lead by LEIS. All four schemes employed the transition $6p^2 \ ^3P_0 - 7s \ ^3P_1^0$ (283.3 nm) as the first step. The four different second step transitions examined are shown

in Table 6 with the enhancement factor (two-step LEI signal /one-step LEI signal) for each. The transition $7s\ ^3P_1^0 \rightarrow 9p\ ^3P_1$ (509.0 nm) was chosen as the second step since the greatest enhancement factor was obtained using this transition.

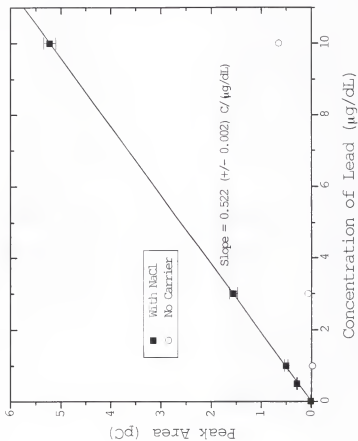
Carrier

The optimized system parameters were found to be the same for lead as they were for Mg. Once all of the optimizations were performed, aqueous solutions of different concentrations of lead were introduced to determine the linearity of the system response. It was observed that at lower concentrations of lead ($<100\ \mu\text{g/dL}$), the linearity of the analytical curve was very poor. Therefore, the feasibility of using a matrix modifier to act as a carrier for the lower concentration samples was evaluated. High purity NaCl was chosen as a possible carrier. A volume of $10\ \mu\text{L}$ sodium chloride solution was injected with each sample. No blank signal was observed for the NaCl. However, an enhancement of the lead ionization signal was observed as well as excellent linearity for aqueous lead concentrations $\leq 10\ \mu\text{g/dL}$, which can be seen in Figure 38. The Log-Log plot for the aqueous lead standards with NaCl (Figure 39) yielded a slope of $0.98 (\pm 0.03)$ and a standard error of the estimates of 0.018 . A slight curvature of the lead signal towards the concentration axis was observed for

Table 6. Enhancement of LEI signal for different two-step excitation schemes for lead

λ_2 (nm)	Transition	Enhancement Factor
498.1	$7s\ ^3P_{1,0} \rightarrow 9p\ ^3D_2$	111
500.5	$7s\ ^3P_{1,0} \rightarrow 9p\ ^3P_1$	37
509.0	$7s\ ^3P_{1,0} \rightarrow 9p\ ^3P_1$	1522
600.2	$7s\ ^3P_{1,0} \rightarrow 8p\ ^3D_2$	194

Figure 38. Analytical curve for aqueous lead standards with and without NaCl addition



concentrations $>10 \mu\text{g/dL}$. It is believed that this signal suppression may be due to chloride interference from the NaCl [162]. Signal suppression due to space charge effects from overloading of the miniature-flame may also contribute. The pronounced nonlinearity of the aqueous lead solutions without NaCl can also be seen from Figure 39.

Lower concentrations of blood lead standards were also introduced to check the linearity of the system response. It was observed that at all of the blood lead concentrations, the analytical curve displayed good linearity as shown in Figure 40. A linear regression of the Log-Log plot for the blood lead standards (Figure 39) yielded a slope of 1.00 (± 0.03) and a standard error of the estimates of 0.030. Therefore, a carrier was not needed and NaCl was not used with the blood samples and standards. It is believed, in this case, that the blood matrix remaining after drying and ashing is vaporized with the lead and acts as a carrier. There was no observable ionization signal from the blood when one or more of the laser beams was blocked. Therefore, there was no observable signal resulting from the ionization of the blood matrix by the laser beams.

Figure 39. Log-Log plot of analytical curves for aqueous lead and blood lead

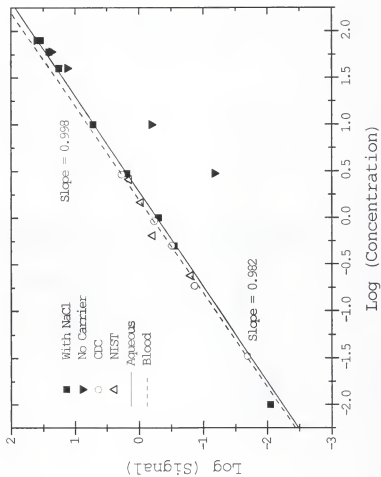
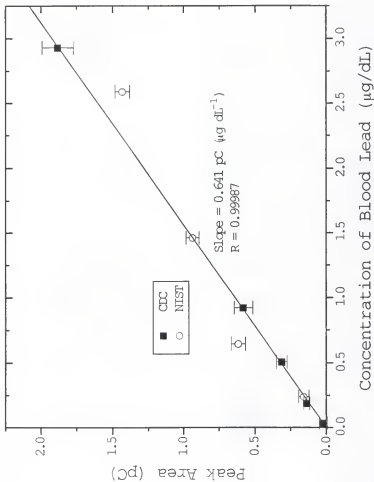


Figure 40. Analytical curve for diluted blood lead standards



Calibration Behavior

The Log-Log plot of the analytical curve for aqueous lead standards containing 100 $\mu\text{g Na/dL}$ is shown in Figure 39. The slope of the analytical curve was found to be 0.522 ± 0.002 $\text{C}/(\mu\text{g/dL})$ with intercept $0 \pm 1 \times 10^{-9}$ C for 5 data points and standard error of the estimates of 0.015. A linear dynamic range of $\sim 10^4$ was found with the upper concentration limited by overloading of the transimpedance amplifier. The lower limiting noise was a result of extraneous rf noise and was measured to be 9.0×10^{-17} C. A detection limit (3σ) for aqueous lead was calculated to be 5.2×10^{-4} $\mu\text{g/dL}$ (52 fg absolute).

The Log-Log plot of the analytical curve for blood lead is also shown in Figure 39. The slope of the analytical curve was found to be 0.641 ± 0.004 $\text{C}/(\mu\text{g/dL})$ with intercept $0 \pm 8 \times 10^{-10}$ C for 5 data points and standard error of the estimates of 0.011. A linear dynamic range of about 10^4 was found with the upper concentration again limited by overloading of the transimpedance amplifier. For diluted blood, a detection limit (3σ) of 4.2×10^{-4} $\mu\text{g/dL}$ (42 fg absolute) was calculated. This corresponds to a detection limit of 8.9×10^{-3} $\mu\text{g/dL}$ (890 fg absolute) for lead in whole blood. This is well below the

CDC's 10 µg/dL level of concern, and would also be useful for substantially lower blood lead concentrations. The higher sensitivity of the blood standards compared to the aqueous standards with NaCl added is most likely a result of the better carrier characteristics of the blood matrix compared to the NaCl.

One human blood sample of unknown lead concentration was also analyzed by graphite furnace-flame-LEIS. A value of 8.7 µg/dL (± 0.3) was calculated from the analytical curve. The human blood sample was also analyzed by Besteman et al. [163] using capacitively coupled microwave plasma atomic emission spectrometry (CCMP-AES). A value of 8.7 µg/dL was also obtained by that method. Therefore, the results obtained by the two independent methods (one using ionization detection and the other optical emission detection) were in good agreement.

CHAPTER 7 CONCLUSIONS

Absolute Analysis

A new burner was designed and used for ETV-FL-LEI of Mg. A two orders of magnitude reduction in the flame noise was obtained with this new miniature burner design. The vaporization, transport, probing, detection, and atomization efficiencies for this new system were measured experimentally for the possibility of absolute analysis. All of the efficiencies, except the vaporization efficiency, were found to be less than unity. For absolute analysis, ideally all of these efficiencies should equal unity.

It was also found that the matrix has a pronounced effect on the transport efficiency as was evident from the need for a carrier (methanol) at low concentrations of Mg. Since a method must be free from matrix interferences to be considered absolute, even if the system efficiencies were improved to unity, the method would still not be considered absolute because of this matrix dependence of the transport efficiency. Therefore, we must conclude that the combination of

electrothermal vaporizer with flame-laser enhanced ionization should not be considered an absolute method.

Pb in Blood

The analysis of lead in a complex sample matrix, blood, was attempted using ETV-flame-LEI. The results obtained show that ETV-flame-LEIS can be readily used for the determination of Pb concentrations in whole blood with minimal sample preparation (21:1 dilution with ultrapure water). ETV temperature programming allowed for sufficient matrix removal to free this method from ionization interferences usually associated with LEIS of real samples. It was also found that the blood matrix that did vaporize with the analyte acted as a very good carrier. Therefore, the addition of a carrier at low Pb concentrations was not necessary. A detection limit of $8.9 \times 10^{-3} \mu\text{g/dL}$ (890 fg absolute) for lead in whole blood was obtained. This compares favorably with other methods currently used to determine blood lead concentrations [12,13].

Future Work

Although ETV-flame-LEI was found to not be suitable for absolute analysis, there still exists the possibility for standardless analysis. If this were to be considered, first

the transport, probing, and detection efficiencies must all be increased to unity. In order to increase the transport efficiency, the ETV-to-burner interface must be redesigned. Possibly, the ETV and burner could be designed as a single unit where there is no tubing between the burner and ETV. To increase the probing efficiency to unity, the laser beam for λ_1 must be expanded to encompass the flame and a higher repetition rate laser (≥ 1 kHz) must be used. To increase the detection efficiency to unity, the laser beams must be positioned as close as possible to the high voltage electrode. The atomization efficiency may be less than unity as long as it remains constant over time. A different flame gas mixture, such as N_2O/air , may be examined in order to improve the atomization efficiency for Mg. After these changes are made and if the efficiencies were improved, the stability of the calibration over time would still need to be established for the possibility for standardless analysis.

Perhaps the most promising area of future work lies in the application of ETV-flame-LEIS to trace element analysis of samples with complex matrices. The analysis of other trace elements in blood could be attempted. Also, the analysis of trace elements in other complex matrices, such as biological tissues, environmental samples, and seawater, could be examined.

REFERENCES

1. L. deGalan and G.F. Samaey, *Anal. Chim. Acta*, **50**, 39 (1970).
2. B. L'vov, *Spectrochim. Acta*, **45B**, 533 (1990).
3. B.W. Smith, G.A. Petrucci, R.G. Badini, and J.D. Winefordner, from *Resonance Ionization Spectroscopy 1988: Proceedings of the Fourth International Symposium on Resonance Ionization Spectroscopy and its Applications held at the National Bureau of Standards, Gaithersburg, MD, from 10-15, April, 1988*, Institute of Physics Publishing, Philadelphia, 1988.
4. B.W. Smith, G.A. Petrucci, R.G. Badini, and J.D. Winefordner, *Anal. Chem.*, **65**, 118 (1993).
5. C.Th.J. Alkemade, Tj. Hollander, W. Snelleman, and P.J.Th. Zeegers, *Metal Vapours in Flames*, Pergamon Press, Oxford (1982).
6. C. Minoia, E. Sabbioni, P. Apostoli, R. Pietra, L. Pozzoli, M. Gallorini, G. Nicolau, L. Alessio, and E. Capoldaglio, *The Science of Total Environment*, **95**, 89 (1990).
7. N. Omenetto and J.D. Winefordner, *Progress Anal. At. Spectrosc.*, **2**, 1 (1979).
8. R.B. Green, R.A. Keller, P.K. Schenck, J.C. Travis, and G.G. Luther, *J. Am. Chem. Soc.*, **98**, 8517 (1976).
9. A.R. Flegal and D.R. Smith, *Environ. Res.*, **58**, 125 (1992).
10. J. Schwartz, C. Angle, and H. Pitcher, *Pediatrics*, **77**, 281 (1986).
11. J. Schwartz and D. Otto, *Arch. Environ. Health*, **42**, 153 (1987).
12. A. Lásztity, M. Viczián, X. Wang, and R.M. Barnes, *J. Anal. At. Spectrom.*, **4**, 761 (1989).

13. J.M. Christensen, O.M. Poulsen, and T. Anglov, *J. Anal. At. Spectrom.*, **7**, 329 (1992).
14. R.B. Green, R.A. Keller, G.G. Luther, P.K. Schenck, and J.C. Travis, *Appl. Phys. Lett.*, **29**, 727 (1976).
15. P.D. Foote and F.L. Mohler, *Phys. Rev.*, **26**, 195 (1925).
16. F.M. Penning, *Physica*, **8**, 137 (1928).
17. R.B. Green, J.C. Travis, and R.A. Keller, *Anal. Chem.*, **48**, 1954 (1978).
18. G.C. Turk, J.C. Travis, J.R. DeVoe, and T.C. O'Haver, *Anal. Chem.*, **50**, 817 (1978).
19. O. Axner and H. Rubinsztein-Dunlop, *Spectrochim. Acta*, **44B**, 835 (1989).
20. J.C. Travis, G.C. Turk, and R.B. Green, *Anal. Chem.*, **54**, 1006A (1982).
21. R.B. Green, G.J. Havrilla, and T.O. Trask, *Appl. Spectrosc.*, **34**, 561 (1980).
22. G.C. Turk, J.C. Travis, J.R. DeVoe, and T.C. O'Haver, *Anal. Chem.*, **51**, 1890 (1979).
23. G.J. Havrilla and R.B. Green, *Anal. Chem.*, **52**, 2376 (1980).
24. G.C. Turk, *Anal. Chem.*, **53**, 1187 (1981).
25. N.J. Szabo, H.W. Latz, G.A. Petrucci, and J.D. Winefordner, *Anal. Chem.*, **63**, 704 (1991).
26. O. Axner and H. Rubinsztein-Dunlop "Fundamental mechanisms of laser-enhanced ionization: the production of ions" from *Laser-Enhanced Ionization Spectrometry*, John Wiley and Sons, Inc., New York, 1996, pp.1-98.
27. J.C. Travis and G.C. Turk "Fundamental mechanisms of laser-enhanced ionization: signal detection" from *Laser-Enhanced Ionization Spectrometry*, John Wiley and Sons, Inc., New York, 1996, pp.99-160.

28. Tj. Hollander, P.J. Kalff, and C.Th.J. Alkemade, *J. Chem. Phys.*, **39**, 2558 (1963).
29. O. Axner, T. Berglind, J.L. Heully, I. Lindgren, and H. Rubinsztein-Dunlop, *J. Appl. Phys.*, **55**, 3215 (1984).
30. O. Axner and S. Sjöström, *Spectrochim. Acta*, **47B**, 245 (1992).
31. O. Axner and P. Ljungberg, *J. Quant. Spectrosc. Radiat. Transfer*, **50**, 277 (1993).
32. P. Ljungberg, D. Boudreau, and O. Axner, *Spectrochim. Acta*, **49B**, 1491 (1994).
33. D. Boudreau, P. Ljungberg, and O. Axner, *Spectrochim. Acta*, **51B**, 413 (1996).
34. M. Sargent, III, M.O. Scully, and W.E. Lamb, Jr., *Laser Physics*, Addison-Wesley, Reading, MA, 1974.
35. J.W. Daily, *Appl. Opt.*, **16**, 2322 (1977).
36. O. Axner and P. Ljungberg, *Spectrochim. Acta Rev.*, **15**, 181 (1993).
37. R. Salomaa and S. Stenholm, *J. Phys. B*, **8**, 1795 (1975).
38. R. Salomaa and S. Stenholm, *J. Phys. B*, **9**, 1221 (1976).
39. R. Salomaa, *J. Phys. B*, **10**, 3005 (1977).
40. R. Salomaa, *Phys. Scr.*, **15**, 251 (1977).
41. M.S. Feld and A. Javan, *Phys. Rev.*, **177**, 540 (1969).
42. Th. Hänsch and P. Toschek, *Z. Phys.*, **236**, 213 (1970).
43. R.G. Brewer and E.L. Hahn, *Phys. Rev. A*, **11**, 1641 (1975).
44. P.R. Berman, *Adv. At. Mol. Phys.*, **13**, 57 (1977).
45. J.H. Eberly, H. Walter, and K.W. Rothe, Eds., *Laser Spectroscopy IV*, Springer-Verlag, Berlin, 1979, pp. 80-87.

46. T.J. McIlrath and J.L. Carsten, *Phys. Rev. A*, **6**, 1091 (1972).
47. O.I. Matveev and N. Omenetto "Some considerations on signal detection and signal to noise ratio in laser enhanced ionization spectroscopy" from *Resonance Ionization Spectroscopy and its Applications held in Bernkastel-Kues, Germany, July 1994*, AIP Press, Inc., Woodbury, NY, 1995.
48. J.C. Travis, G.C. Turk, J.R. DeVoe, P.K. Schenck and C.A. van Dijk, *Prog. Anal. At. Spectrosc.*, **7**, 199 (1984).
49. G.J. Havrilla, P.K. Schenck, J.C. Travis, and G.C. Turk, *Anal. Chem.*, **56**, 186 (1984).
50. J.C. Travis, in *Analytical Laser Spectroscopy* (S. Martellucci and A.N. Chester, eds.), NATO ASI Ser. B, Vol. 119, Plenum Press, New York, 1985, p. 213.
51. T. Kántor, *Spectrochim. Acta*, **43B**, 1299 (1988).
52. N.A. Fuchs and A.G. Stutugin, *Highly Dispersed Aerosols*, Ann Arbor Science, London, 1970.
53. D.T. Shaw, ed., *Fundamentals of Aerosol Science*, Wiley, New York, 1978.
54. D.T. Shaw, ed., *Recent Developments in Aerosol Science*, Wiley, New York, 1978.
55. S.K. Friedlander "Aerosol dynamics and gas-to-particle conversion" from *Recent Developments in Aerosol Science* (D.T. Shaw, ed.), Wiley, New York, 1978.
56. W. Slavin, D.C. Manning, and G.R. Carnick, *At. Spectrosc.*, **2**, 137 (1981).
57. L. deGalan and J.D. Winefordner, *J. Quant. Spectrosc. Radiat. Transfer*, **7**, 251 (1967).
58. Yu.K. Akimov, O.V. Igatiev, A.I. Kalinin, and V.F. Kushniruk, *Semiconductor Detectors In Experimental Physics*, Energoatomizdat, Moscow, 1989.
59. N. Omenetto, G.C. Turk, M. Rutledge, and J.D. Winefordner, *Spectrochim. Acta*, **42B**, 807 (1987).

60. N. Omenetto, B.W. Smith, P.B. Farnsworth, and J.D. Winefordner, *J. Anal. Atom. Spectrom.*, **7**, 89 (1992).
61. J.C. Travis, *J. Chem. Educ.*, **59**, 909 (1982).
62. G.C. Turk "Analytical performance of laser-enhanced ionization in flames" from *Laser-Enhanced Ionization Spectrometry*, John Wiley and Sons, Inc., New York, 1996, pp. 161-211.
63. N. Omenetto, B.W. Smith, and L.P. Hart, *Fresenius' Z. Anal. Chem.*, **324**, 683 (1986).
64. G.J. Havrilla and C.C. Carter, *Appl. Opt.*, **26**, 3510 (1987).
65. G.C. Turk, J.C. Travis, and J.R. DeVoe, *Anal. Chem.*, **51**, 1890 (1979).
66. O. Axner, I. Magnusson, J. Petersson, and S. Sjöström, *Appl. Spectrosc.*, **41**, 19 (1987).
67. J.D. Messman, N.E. Schmidt, J.D. Parli, and R.B. Green, *Appl. Spectrosc.*, **39**, 504 (1985).
68. G.C. Turk, J.R. DeVoe, and J.C. Travis, *Anal. Chem.*, **54**, 643 (1982).
69. N.V. Chekalin and I.I. Vlasov, *J. Anal. At. Spectrom.*, **7**, 225 (1992).
70. O. Axner, I. Lindgren, I. Magnusson, and H. Rubinsztein-Dunlop, *Anal. Chem.*, **57**, 776 (1985).
71. A.A. Gorbatenko, N.B. Zorov, S.Yu. Karopova, Yu.Ya. Kuzyakov, and V.I. Chaplygin, *J. Anal. At. Spectrom.*, **3**, 527, (1988).
72. G.C. Turk and M. De-Ming, *NBS Spec. Publ. (U.S.)*, **260-106**, 30-33 (1986).
73. Yu.Ya. Kuzyakov, N.B. Zorov, V.I. Chaplygin, and A.A. Gorbatenko, in *Resonance Ionization Spectroscopy 1988 (Proceedings of the 4th International Symposium on Resonance Ionization Spectroscopy and Its Applications)* (T.B. Lucatorto and J.E. Parks, eds.), pp.179-182, IOP Publishing Bristol, 1989.

74. G.C. Turk, W.G. Mallard, P.K. Schenck, and K.C. Smyth, *Anal. Chem.*, **51**, 2408 (1979).
75. G.J. Havrilla, S.J. Weeks, and J.C. Travis, *Anal. Chem.*, **54**, 2566 (1982).
76. J.C. Travis, G.C. Turk, R.B. Green, *ACS Symp. Ser.*, **85**, 91-101 (1978).
77. O. Axner and H. Rubinsztein-Dunlop, *Appl. Opt.*, **32**, 867 (1993).
78. V.I. Chaplygin, Yu.Ya. Kuzyakov, and O.A. Novodvorsky, *Talanta*, **34**, 191 (1987).
79. V.I. Chaplygin, N.B. Zorov, and Yu.Ya. Kuzyakov, *Talanta*, **30**, 505 (1983).
80. N.B. Zorov, Yu.Ya. Kuzyakov, O.I. Matveev, and V.I. Chaplygin, *J. Anal. Chem. USSR (Engl. Transl.)*, **35**, 1108 (1980).
81. I.V. Bykov, A.B. Skvortsov, Yu.G. Tatsii, and N.V. Chekalin, *J. Phys. (Paris), Colloq.*, **C7**, 345 (1983).
82. R.W. Fox, C.S. Weimer, L. Hollberg, and G.C. Turk, *Spectrochim. Acta Rev.*, **15**, 291 (1993).
83. J.E. Hall and R.B. Green, *Anal. Chem.*, **55**, 1811 (1983).
84. N.B. Zorov, Yu.Ya. Kuzyakov, and O.I. Matveev, *Zh. Anal. Khim.*, **37**, 520 (1982).
85. A.G. Marunkov and N.V. Chekalin, *J. Anal. Chem. USSR (Engl. Transl.)*, **42**, 506 (1987).
86. R.B. Green and J.E. Hall, *J. Phys. (Paris), Colloq.*, **C7**, 317 (1983).
87. N.V. Chekalin, V.I. Pavlutsкая, and I.I. Vlasov, *Spectrochim. Acta*, **46B**, 1701 (1991).
88. L.E. Salcedo Torres, N.B. Zorov, and Yu.Ya. Kuzyakov, *J. Anal. Chem. USSR (Engl. Transl.)*, **36**, 1016 (1981).
89. O.I. Matveev, P. Cavalli, and N. Omenetto, in *Resonance Ionization Spectroscopy 1994 (Proceedings of the 7th International Symposium on Resonance Ionization*

Spectroscopy and Its Applications) (H.J. Kluge, J.E. Parks, and K. Wendt, eds.), pp. 269-272, AIP Press, New York, 1995.

90. L.C. Chandola and P.P. Khanna, *Spectrochim. Acta*, **48A**, 1547 (1992).
91. O.I. Matveev, *J. Anal. Chem. USSR (Engl. Transl.)*, **43**, 944 (1988).
92. G.C. Turk, J.C. Travis, and J.R. DeVoe, *J. Phys. (Paris), Colloq.*, **C7**, 301 (1983).
93. L.C. Chandola, P.P. Khanna, and M.A.N. Razvi, *Anal. Lett.*, **24**, 1685 (1991).
94. A.S. Gonchakov, N.B. Zorov, Yu.Ya. Kuzyakov, and O.I. Matveev, *Anal. Lett.*, **12**, 1037 (1979).
95. D.J. Ehrlich, R.M. Osgood, Jr., G.C. Turk, and J.C. Travis, *Anal. Chem.*, **52**, 1354 (1980).
96. Y. Yan, D. Ding, Z. Zhang, S. Jin, and Q. Jin, *Guangpuxue Yu Guangpu Fenxi*, **4**, 1 (1984).
97. P. Zhang, J. Du, J. He, and H. Li, *Fenxi Huaxue*, **10**, 66 (1985).
98. M.D. Seltzer and R.B. Green, *Appl. Spectrosc.*, **43**, 257 (1989).
99. L.P. Hart, B.W. Smith, and N. Omenetto, *Spectrochim. Acta*, **40B**, 1637 (1985).
100. N. Omenetto, T. Berthoud, P. Cavalli, and G. Rossi, *Anal. Chem.*, **57**, 1256 (1985).
101. G.J. Havrilla and K.J. Choi, *Anal. Chem.*, **58**, 3095 (1986).
102. S.J. Weeks, H. Haraguchi, and J.D. Winefordner, *J. Quant. Spectrosc. Radiat. Transfer*, **19**, 633 (1978).
103. K.C. Smyth and W.G. Mallard, *Combust. Sci. Technol.*, **26**, 35 (1981).
104. G.C. Turk and H.M. Kingston, *J. Anal. At. Spectrom.*, **5**, 595 (1990).

105. K.S. Epler, T.C. O'Haver, G.C. Turk, and W.A. MacCrehan, *Anal. Chem.*, **60**, 2062 (1988).
106. B.V. L'vov, *Atomic Absorption Spectrochemical Analysis*, American Elsevier, New York, 1970.
107. J.C. Travis, M. Epstein, P.K. Schenck, G.C. Turk, D.M. Sweger, and J.R. DeVoe, *Proc. Colloq. Spectrosc. Int. 20th, and Int. Conf. At. Spectrosc. 7th*, Prague, 118 (1977).
108. A.G. Marunkov, T.V. Reutova, and N.V. Chekalin, *Zh. Anal. Khim.*, **41B**, 681 (1986).
109. N.V. Chekalin, A.G. Marunkov, V.I. Pavlutsкая, and S.V. Bachin, *Spectrochim. Acta*, **46B**, 551 (1991).
110. O. Axner, M. Lejon, I. Magnusson, H. Rubinsztein-Dunlop, and S. Sjöström, *Appl. Opt.*, **26**, 3521 (1987).
111. J. Du, H. Li, L. Pan, H. Chen, J. Lian, C. Jin, C. Wang, and P. Zhang, *Fenxi Huaxue*, **18**, 607 (1990).
112. G.C. Turk, G.J. Havrilla, J.D. Webb, and A.R. Forster, *Anal. Chem. Symp. Ser.*, **19**, 63 (1984).
113. N.V. Chekalin, V.I. Pavlutsкая, and I.I. Vlasov, *Conf. Ser.-Inst. Phys.*, **114**, 283 (1991).
114. O. Axner, M. Norberg, M. Persson, and H. Rubinsztein-Dunlop, *Appl. Spectrosc.*, **44**, 1117 (1990).
115. K.L. Riter, O.I. Matveev, B.W. Smith, and J.D. Winefordner, *Anal. Chim. Acta*, in Press (1996).
116. A. Miyazaki and H. Tao, *J. Anal. At. Spectrom.*, **6**, 173 (1991).
117. H.M. Kingston, I.L. Barnes, T.J. Brady, T.C. Rains, and M.A. Champ, *Anal. Chem.*, **50**, 2064 (1978).
118. G.C. Turk, W.A. MacCrehan, K.S. Epler, and T.C. O'Haver, *Conf. Ser.-Inst. Phys.*, **94**, 327 (1989).
119. K.S. Epler, T.C. O'Haver, and G.C. Turk, *J. Anal. At. Spectrom.*, **9**, 79 (1994).
120. S.C. Wang and K.C. Lin, *Anal. Chem.*, **66**, 2180 (1994).

121. R.B. Green "Applications of laser-enhanced ionization spectrometry" from *Laser-Enhanced Ionization Spectrometry*, John Wiley and Sons, Inc., New York, 1996, pp.213-232.
122. N.B. Zorov "Nonflame reservoirs for laser-enhanced ionization spectrometry" from *Laser-Enhanced Ionization Spectrometry*, John Wiley and Sons, Inc., New York, 1996, pp.233-263.
123. A.S. Gonchakov, N.B. Zorov, Yu.Ya. Kuzyakov, and O.I. Matveev, *Zh. Anal. Khim.*, **34**, 2312 (1979).
124. L.E. Salsedo Torres, Ph.D. thesis, Moscow State University (1981).
125. I. Magnusson, O. Axner, I. Lindgren, and H. Rubinsztein-Dunlop, *Appl. Spectrosc.*, **40**, 968 (1986).
126. I. Magnusson, S. Sjöström, M. Lejon, and H. Rubinsztein-Dunlop, *Spectrochim. Acta*, **42B**, 713 (1987).
127. I. Magnusson, *Spectrochim. Acta*, **43B**, 727 (1988).
128. S. Sjöström, I. Magnusson, M. Lejon, and H. Rubinsztein-Dunlop, *Anal. Chem.*, **60**, 1629 (1988).
129. D.J. Butcher, R.L. Irvin, S. Sjöström, A.P. Walton, and R.B. Michel, *Spectrochim. Acta*, **46B**, 9 (1991).
130. V.I. Chaplygin, N.B. Zorov, Yu.Ya. Kuzyakov, and O.I. Matveev, *Zh. Anal. Khim.*, **38**, 802 (1983).
131. A. Miyazaki and H. Tao, *Anal. Sci.*, **7**, 1053 (1991).
132. B.W. Smith, G.A. Petrucci, R.G. Badini, and J.D. Winefordner, *Anal. Chem.*, **65**, 118 (1993).
133. K.L. Riter, W.L. Clevenger, L.S. Mordoh, B.W. Smith, O.I. Matveev, and J.D. Winefordner, *J. Anal. At. Spectrom.*, **11**, 393 (1996).
134. A.G. Marunkov, Ph.D. thesis, Moscow State University (1989).
135. N.V. Chekalin, A. Khalmanov, A.G. Marunkov, I.I. Vlasov, Y. Malmsten, O. Axner, V.S. Dorofeev, and E.

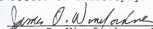
- Glukhan, *Spectrochim. Acta*, **50B**, 753 (1995).
136. G.C. Turk and R.L. Watters, *Anal. Chem.*, **57**, 1979 (1985).
 137. G.C. Turk, L. Yu, R.L. Watters, and J.C. Travis, *Appl. Spectrosc.*, **46**, 1217 (1992).
 138. K.C. Ng, M.J. Angebrann, and J.D. Winefordner, *Anal. Chem.*, **62**, 2506 (1990).
 139. L. Yu, S.R. Koirtyohann, G.C. Turk, and M.L. Salit, *J. Anal. At. Spectrom.*, **9**, 997 (1994).
 140. G.C. Turk, L. Yu, and S.R. Koirtyohann, *Spectrochim. Acta*, **49B**, 1537 (1994).
 141. G.C. Turk, L. Yu, and S.R. Koirtyohann, from *Resonance Ionization Spectroscopy 1994: Proceedings of the Seventh International Symposium on Resonance Ionization Spectroscopy and its Applications held in Bernkastel-Kues, Germany, July 1994*, AIP Press Inc., Woodbury, NY, 1995.
 142. A.A. Gorbatenko, Yu.Ya. Kuzyakov, A.R. Murtazin, and N.B. Zorov, from *Resonance Ionization Spectroscopy 1994: Proceedings of the Seventh International Symposium on Resonance Ionization Spectroscopy and its Applications held in Bernkastel-Kues, Germany, July 1994*, AIP Press Inc., Woodbury, NY, 1995.
 143. M.E. Churchwell, T. Beeler, J.D. Messman, and R.B. Green, *Spectrosc. Lett.*, **18**, 679 (1985).
 144. Yu.Ya. Kuzyakov, O.I. Matveev, and O.A. Novodvorskii, *Zh. Prikl. Spektrosk.*, **40**, 145 (1984).
 145. L.S. Ornstein and H. Brinkman, *K. Acad. Wet. Amsterdam Proc.*, **34**, 33 (1931).
 146. L.S. Ornstein and H. Brinkman, *Physica (Amsterdam)*, **1**, 797 (1934).
 147. G.F. Kirkbright, M.K. Peters, M. Sargent, and T.S. West, *Talanta*, **15**, 663 (1968).
 148. N. Omenetto, G.C. Turk, M. Rutledge, and J.D. Winefordner, *Spectrochim. Acta*, **42B**, 807 (1987).

149. N. Omenetto, B.W. Smith, P.B. Farnsworth, and J.D. Winefordner, *J. Anal. At. Spectrom.*, **7**, 89 (1992).
150. J.D. Winefordner and T.J. Vickers, *Anal. Chem.*, **36**, 161 (1964).
151. S.M. Schmertmann, S.E. Long, and R.F. Browner, *J. Anal. At. Spectrom.*, **2**, 687 (1987).
152. A.B. Gillespie, in *Signal, Noise, and Resolution in Nuclear Counter Amplifiers*, McGraw-Hill, New York, 1953.
153. M.P. Escobar, B.W. Smith, and J.D. Winefordner, *Anal. Chim. Acta*, **320**, 11 (1996).
154. K.C. Ng and J.A. Caruso, *Anal. Chim. Acta*, **143**, 209 (1982).
155. E. Hoffman, C. Lüdke, and H. Scholze, *J. Anal. At. Spectrom.*, **9**, 1237 (1994).
156. Perkin-Elmer Corp. Analytical Techniques for Graphite Furnace Atomic Absorption Spectrometry. Publication No. B332; Perkin-Elmer Corp.: Norwalk, CT, 1984.
157. J.R. Fuhr, G.A. Martin, and W.L. Wise, *J. Phys. Chem. Refer. Data*, **17**(4), 1 (1988).
158. L. deGalan, R. Smith, and J.D. Winefordner, *Spectrochim. Acta*, **23B**, 521 (1968).
159. W.L. Wiese, M.W. Smith, and B.M. Miles, *Atomic Transition Probabilities-Volume II. Sodium through Calcium*, NSRDS, Washington, D.C., 1969.
160. J.D. Ingle Jr. and S.R. Crouch, *Spectrochemical Analysis*, Prentice Hall, Englewood Cliffs, NJ, 1988.
161. W.P. Townsend, D.S. Smyly, P.J.Th. Zeegers, V. Svoboda, and J.D. Winefordner, *Spectrochim. Acta*, **26B**, 595 (1971).
162. J.M. Shekiri Jr., R.K. Skogerboe, and H.E. Taylor, *Anal. Chem.*, **60**, 2578 (1988).
163. A.D. Besteman, N. Lau, D.-Y. Liu, B.W. Smith, and J.D. Winefordner, *J. Anal. At. Spectrom.*, **11**, 479 (1996).

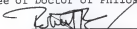
BIOGRAPHICAL SKETCH

Ken Riter was born on May 14, 1970, in Sioux Falls, SD. He graduated from Washington Senior High School in Sioux Falls, SD, in May, 1988. In May, 1992, he graduated from Saint Olaf College in Northfield, MN, with a Bachelor of Arts degree in chemistry. In August, 1992, he entered the Graduate School at the University of Florida in Gainesville, FL.

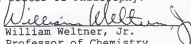
I certify that I have read this study and that in my opinion it conforms to acceptable standards of scholarly presentation and is fully adequate, in scope and quality, as a dissertation for the degree of Doctor of Philosophy.


James D. Winefordner, Chair
Graduate Research Professor
of Chemistry


I certify that I have read this study and that in my opinion it conforms to acceptable standards of scholarly presentation and is fully adequate, in scope and quality, as a dissertation for the degree of Doctor of Philosophy.


Robert P. Kennedy
Associate Professor of
Chemistry


I certify that I have read this study and that in my opinion it conforms to acceptable standards of scholarly presentation and is fully adequate, in scope and quality, as a dissertation for the degree of Doctor of Philosophy.


William Weltner, Jr.
Professor of Chemistry

I certify that I have read this study and that in my opinion it conforms to acceptable standards of scholarly presentation and is fully adequate, in scope and quality, as a dissertation for the degree of Doctor of Philosophy.


Eric R. Allen
Professor of Environmental
Engineering Sciences

I certify that I have read this study and that in my opinion it conforms to acceptable standards of scholarly presentation and is fully adequate, in scope and quality, as a dissertation for the degree of Doctor of Philosophy.


Michael D. Annable
Assistant Professor of
Environmental Engineering
Sciences

LD
1780
1996
.R598

